

Conformal Tradeoffs: Guarantees Beyond Coverage

Petrus H. Zwart

PHZwart@lbl.gov

Center for Advanced Mathematics in Energy Research Applications, Berkeley Synchrotron Infrared Structural Biology Program, & Molecular Biophysics and Integrated Bioimaging Division, 1 Cyclotron Road, Berkeley, CA 94720, USA

Abstract

Deployed conformal predictors are long-lived decision infrastructure operating over finite operational windows. The real-world question is not merely “Does the true label lie in the prediction set at the target rate?”, i.e. marginal coverage, but “How often does the deployed system commit versus defer? What error exposure does it induce when it acts? How do these operational rates trade off?” Marginal coverage does not summarize these deployment-facing quantities: the same calibrated thresholds can yield very different operational profiles depending on score geometry.

This paper provides a framework for operational certification and planning beyond coverage. We make three contributions. (1) Small-Sample Beta Correction (SSBC): We invert the exact finite-sample Beta/rank law for split conformal to map a user coverage request (α^*, δ) into a concrete calibrated grid point with PAC-style semantics, providing explicit finite-window coverage guarantees for the deployed rule. (2) Calibrate-and-Audit: Because no distribution-free pivot exists for rates beyond coverage, we introduce a two-stage design: an independent audit set yields a reusable region–label table that supports certified finite-window predictive envelopes (Binomial/Beta–Binomial) for operational quantities—commitment frequency, deferral, decisive error exposure, commit purity—or related quantities via linear projection, without committing to a specified scalar objective. (3) Geometric characterization: We expose the feasibility constraints, regime boundaries (hedging vs. rejection), and cost-coherence conditions induced by a fixed conformal partition, explaining why operational rates are coupled and how calibration navigation trades them off.

The output is an auditable operational menu: given a scoring model, the framework traces the Pareto frontier of attainable operational profiles across calibration settings and attaches finite-window uncertainty envelopes to each regime. We demonstrate the approach on Tox21 toxicity prediction (12 endpoints) and aqueous solubility screening of lipophilic drug candidates via the AquaSolDB dataset.

1 Introduction: deployment-facing conformal prediction

Many classifiers are deployed as long-lived decision infrastructure rather than one-off prediction engines. A single trained scoring model is integrated into downstream workflows and reused over finite operational windows. In this regime, the deployed object is not the score function alone, but the *rule*: (scoring model, one-time calibration procedure, and downstream action convention). The observables that matter to stakeholders are finite-window *operational rates*: how often the system commits versus defers/abstains, and—conditional on commitment—the decisive error exposure and purity induced by attached actions (cf. rejection options and selective classification (Chow, 1970)). These realized rates drive resource planning, safety and compliance, and near-term impact.

Conformal prediction (Vovk et al., 2005; Shafer & Vovk, 2008) is a natural starting point for deployment-facing calibration: it sets score thresholds on held-out data and yields finite-sample, distribution-free *coverage* under exchangeability (Papadopoulos et al., 2002). Coverage, however, is not an operational specification. Once a deployment convention is fixed (e.g., “commit on singletons, defer on hedges or empty sets”), the realized operational profile depends on how calibration choices partition score space and how mass and labels

populate the induced regions. As a result, two conformal rules with identical marginal coverage can behave very differently in deployment.

1.1 The gap: coverage does not determine operational behavior

Standard conformal guarantees that the true label lies in the prediction set at the target coverage rate (under exchangeability). But *coverage alone does not determine the operational profile* of a deployed conformal rule. In particular, different calibrated predictors with the same nominal coverage can exhibit markedly different:

- **Commitment vs. deferral:** the frequency of singleton outputs (and thus decisive actions) versus hedges/abstentions.
- **Decisive error exposure:** the error rate *among committed predictions*, which is the error that “escapes” deferral mechanisms.
- **Trade-off coupling:** improving one operational rate (e.g., reducing deferral) may force degradation in another (e.g., increasing decisive error), with couplings determined by the score distribution geometry rather than by coverage alone.

These are first-order questions for operational readiness and trust calibration, yet they are not easily answered by coverage certificates alone.

1.2 Our approach: calibrate, expose geometry, and audit once

We study a single deployed split-conformal rule through a calibration-conditional, certification-style lens. A calibration choice fixes cutpoints on the score axis, inducing a finite partition of score/output space into regions with set-valued outcomes (e.g., singleton, hedge, abstain). The key device in this paper is to make this *intermediate geometry* explicit and auditable: once the region partition is fixed, many policy- and Key Performance Indicator (KPI)-specific rates are obtained by simple projection from the joint region-label masses. This supports trade-off analysis across calibration settings and enables distribution-free uncertainty statements about *future realized finite-window rates* for the deployed rule.

Figure 1 previews the main object produced by this paper: an auditable operational menu mapping calibration settings to certified finite-window operational profiles, together with a Pareto filter that highlights nondominated operating regimes.

1.3 Contributions

This paper makes operational quantities first-class objects of certification and exploration for deployed conformal predictors. Our contributions are:

(1) Coverage semantics via Small-Sample Beta Correction (SSBC). We invert the exact finite-sample rank/Beta law for split conformal (Marques, 2025) to map a user request (α^*, δ) (e.g., “90% coverage with 90% confidence”) to the least conservative split-conformal grid point satisfying a PAC-style tail constraint:

$$\mathbb{P}_{\mathcal{D}_{\text{cal}}}\left(\mathbb{P}(Y \in \hat{C}(X) \mid \mathcal{D}_{\text{cal}}) \geq 1 - \alpha^*\right) \geq 1 - \delta.$$

This provides an explicit, auditable finite-sample coverage guarantee for the deployed rule and serves as a semantic anchor for subsequent operational navigation. In the binary class-conditional case, SSBC collapses a four-dimensional user specification into a two-dimensional calibration coordinate, simplifying trade-off exploration.

(2) Calibrate-and-Audit for operational certification beyond coverage. Operational rates such as commitment, deferral, and decisive error exposure are not rank-determined and therefore do not admit a conformal “coverage-style” pivot. We introduce a two-stage design:

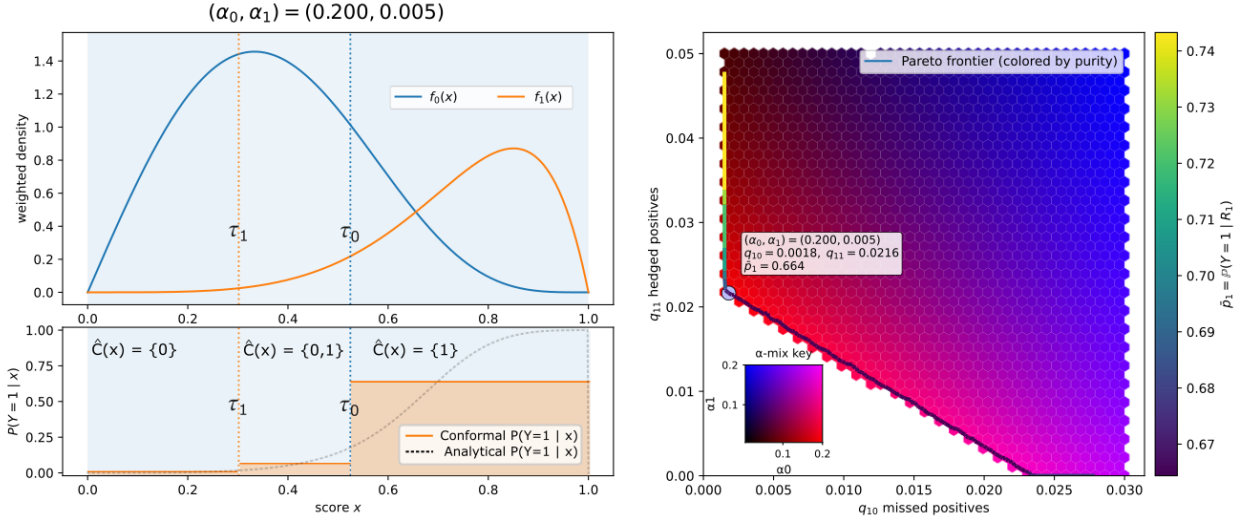


Figure 1: **Operational menu induced by a calibrated conformal rule on a synthetic model.** Left: a calibration choice fixes score cutpoints that partition score space into set-valued outcomes (e.g., singleton, hedge, abstain) and associated region–label probabilities. A deployment convention determines which outcomes trigger commitment versus deferral. Right: sweeping calibration settings traces the attainable set of selected operational rates; the oriented Pareto frontier highlights nondominated operating regimes.

- **Calibrate:** fix thresholds on \mathcal{D}_{cal} , inducing a region partition R_τ .
- **Audit:** use an independent exchangeable set $\mathcal{D}_{\text{audit}}$ to estimate the joint region–label table $\{p_{r,y}\}$.

The joint table is a reusable sufficient statistic: a wide class of operational KPIs are linear projections (or monotone transforms) of $\{p_{r,y}\}$. This model, via an induced Binomial/Beta–Binomial sampling model of events of interest, yields exact finite-window predictive envelopes for future realized operational rates, enabling certified policy comparison across many calibration settings without re-auditing. We also provide a conservative leave-one-out proxy for single-sample settings (Appendix D).

(3) Geometry and feasibility of operational trade-offs. We expose how a fixed conformal partition couples attainable operational rates. In the binary probability-normalized case:

- **Regime boundaries:** the sum $\tau_0 + \tau_1$ determines whether the system can hedge ($\tau_0 + \tau_1 > 1$) or must reject ($\tau_0 + \tau_1 < 1$), inducing sharp transitions in attainable profiles (Section 4).
- **Conservation constraints:** varying thresholds reallocates mass across regions, explaining structural trade-offs between commitment and decisive error exposure.
- **Cost coherence:** we derive compatibility conditions between region-based action conventions and scalar cost models, in advance of any cost model specification that are linear transformations of the auditable primitives (Appendix F).

Together, these results explain *why* some desired operational profiles are infeasible, and provide better guidance for practitioners to navigate emergent trade-offs induced by conformal calibration choices.

1.4 Positioning and related work

Conformal prediction constructs set-valued predictors with finite-sample coverage guarantees under exchangeability (Vovk et al., 2005; Shafer & Vovk, 2008; Angelopoulos & Bates, 2023). Conformal risk control

(CRC) generalizes this viewpoint by selecting thresholds to satisfy user-specified *scalar* risk constraints under related assumptions (Angelopoulos et al., 2024; Bates et al., 2021), and extensions address covariate shift via reweighting or adaptation (Tibshirani et al., 2019; Fannjiang et al., 2022). Recent work also connects conformal methods to downstream decision-making: conformal decision theory calibrates decision rules (often online) to control realized risk (Lekeufack et al., 2023), and decision-theoretic foundations motivate conformal sets as uncertainty objects for risk-averse agents (Kiyani et al., 2025).

Our focus is complementary. Rather than guaranteeing coverage or a single scalar risk functional, we certify finite-window operational rate vectors for a fixed deployed rule and support multi-objective exploration without committing to a scalar objective. The audited primitive is the intermediate geometry induced by calibration—the region partition and its joint region–label table—from which many deployment policies and KPIs follow by projection.

Closest in spirit to our “menu” viewpoint is the inverse CRC of Zhou & Zhu (2025), who trace certified miscoverage–regret trade-offs across robustness levels for predict-then-optimize pipelines; they audit coverage and regret as the downstream objects of interest. In our work, however, we target an earlier deployment stage, where the cost model and operational targets are not yet fixed. At that stage we audit and certify operational quantities—commit and deferral rates, error exposure, purity, and workload—and their 95% predictive envelopes that directly govern resource usage and risk over finite windows.

A different line of work optimizes *efficiency* by selecting, from a family of candidate models, the conformal predictor that minimizes a set-size functional (e.g., interval length/volume, or prediction-set *cardinality* in classification) subject to validity constraints (Yang & Kuchibhotla, 2021). This is well-motivated when downstream utility is monotone in set size. Our objective differs: in many deployments, smaller cardinality does not necessarily imply higher utility, nor lower uncertainty in the induced region-conditional label frequencies. In particular, aggressive singleton behavior can reduce average set size while increasing “decisive error exposure” and degrading the operational profile that stakeholders ultimately care about. When organizational priorities are still being determined, a set size proxy might not be informative enough to guide decision-making. Accordingly, we treat conformal sets as instruments whose value is expressed through a vector of auditable KPIs, and we certify the feasible trade-offs among these rates in finite windows.

1.5 Roadmap

Section 2 formalizes the calibration-conditional viewpoint for a fixed deployed object and defines the region–label table as the auditable primitive. Section 3 presents SSBC and the Calibrate-and-Audit framework, yielding certified finite-window envelopes for operational rates and Pareto-based trade-off navigation. Section 4 characterizes regime boundaries and feasibility constraints induced by the conformal partition. Section 5 validates the framework empirically on Tox21 toxicity prediction and aqueous solubility prediction, and Section 6 discusses limitations and extensions (multiclass, online adaptation, and distribution shift).

2 Setting and notation: calibration-conditional viewpoint

We study a *single deployed predictor* produced by (i) training a scoring model on a training set and then treating it as fixed, followed by (ii) a one-time split conformal calibration on an exchangeable calibration sample. Accordingly, all randomness in our analysis is over the one-time calibration draw and future deployment data; we do not analyze variability due to retraining or repeated recalibration. Later, to make operational rates beyond coverage auditable with certified finite-sample guarantees, we introduce a separate exchangeable *audit set* held out alongside the calibration sample.

2.1 Data splits and exchangeability assumptions

Let $\mathcal{D}_{\text{train}}$ denote a training dataset used to fit a base scoring model, for instance a probabilistic classifier (Goodfellow et al., 2016). After training, the resulting score function is treated as fixed.

Let

$$\mathcal{D}_{\text{cal}} = \{(X_i^c, Y_i^c)\}_{i=1}^{n_{\text{cal}}}, \quad \mathcal{D}_{\text{audit}} = \{(X_i^a, Y_i^a)\}_{i=1}^{n_{\text{audit}}}.$$

The calibration sample \mathcal{D}_{cal} is used once to set the deployed rule’s thresholds; the audit sample $\mathcal{D}_{\text{audit}}$ is held out (e.g., by splitting the calibration pool) and reserved for measuring operational quantities after thresholds are fixed, and is not used to choose thresholds. This approach is equivalent to the double calibration set approach of Yang & Kuchibhotla (2021).

We assume calibration, audit, and future deployment examples are jointly exchangeable (conditional on the fixed trained scoring model). This is the standard split conformal assumption that yields distribution-free finite-sample validity for coverage, and it is the only distributional condition used throughout. All guarantees are scoped to this exchangeable setting; we do not consider covariate or label shift in this paper. In this work we focus on binary classification to isolate the core principles and trade-offs in the clearest setting; extensions to richer output spaces are left for future work.

2.2 Scores and calibration thresholds

Let $\mathcal{Y} = \{1, \dots, K\}$, and let $s : \mathcal{X} \times \mathcal{Y} \rightarrow \mathbb{R}$ denote a nonconformity (score) function (Shafer & Vovk, 2008; Lei et al., 2018). A common choice for probabilistic-like classifiers is $s(x, y) = 1 - P(y | x)$. While this specific form is not required for the present section, it is used in the examples throughout the paper.

Given \mathcal{D}_{cal} , compute calibration nonconformity scores

$$S_i := s(X_i^c, Y_i^c), \quad i = 1, \dots, n_{\text{cal}},$$

and let $S_{(1)} \leq \dots \leq S_{(n_{\text{cal}})}$ denote the sorted values. Split conformal calibration selects a threshold as an order statistic (Papadopoulos et al., 2002; Vovk, 2012a)

$$\tau := S_{(k)},$$

where the index $k \in \{1, \dots, n_{\text{cal}}\}$ is determined by the desired miscoverage level α^* (up to deterministic tie-breaking). It is often convenient to parameterize the same grid by the miscoverage index $u := n_{\text{cal}} + 1 - k$, corresponding to the discrete miscoverage level $\alpha_{\text{grid}} = u / (n_{\text{cal}} + 1)$.

We use *class-conditional* split conformal throughout (Vovk, 2012a;b), where thresholds τ_y are computed separately from calibration scores restricted to $Y_i = y$. The pooled split conformal convention is recovered as the special case with shared thresholds across classes, i.e., $\tau_y \equiv \tau$ for all y .

The key operational point is that, given $(\mathcal{D}_{\text{cal}}, \alpha^*)$, calibration produces a vector of class-conditional thresholds $\tau = (\tau_1, \dots, \tau_K)$, and these thresholds are then held fixed throughout deployment.

2.3 Regions, observability, and policies

Once thresholds are fixed, they induce a finite discrete region by recording which threshold inequalities are satisfied. In the multiclass case it is convenient to write the score vector

$$s(x) := (s(x, 1), \dots, s(x, K))$$

and (optionally class-conditional) thresholds

$$\tau := (\tau_1, \dots, \tau_K),$$

with $\tau_y \equiv \tau$ in the pooled case. The region map is defined by

$$R_\tau(x) := (\mathbf{1}\{s(x, 1) \leq \tau_1\}, \dots, \mathbf{1}\{s(x, K) \leq \tau_K\}) \in \{0, 1\}^K.$$

Thus calibration fixes a region map $R_\tau : \mathcal{X} \rightarrow \{0, 1\}^K$, i.e., a finite partition of score space used throughout deployment. The map R_τ is determined entirely by τ . However, the induced distribution of class labels Y given the region $R_\tau(X)$ —which regions carry mass and how much—depends on the deployment data-generating process. This discrete region partitioning is our decision and exploration interface.

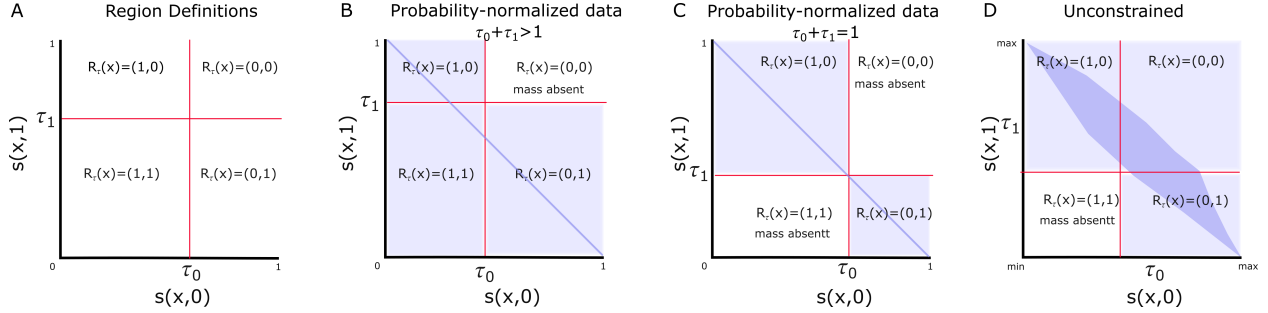


Figure 2: Region definitions and region mass under different data regimes. (A) Thresholds τ_0, τ_1 induce a finite region partition $R_\tau(x)$ independent of data and policy. (B–C) Under probability-normalized scores, data support is restricted to the diagonal, determining which regions carry nonzero mass for different threshold configurations. (D) With unconstrained scores, all regions may carry mass. No deployment policy is applied in this figure.

Operationally, deployment is observed through the joint process $(R_\tau(X), Y)$. All quantities considered in this paper are functions of region frequencies and region-conditioned label composition under fixed thresholds. We treat region identity as the auditable primitive; within-region heterogeneity is intentionally not modeled in this framework. Accordingly, observations that share the same realized region label $R_\tau(X) = r$ are treated as exchangeable for the purpose of estimation and certification.

To formally link regions to downstream consequences, we introduce the concept of a deployment policy. A deployment policy π maps a realized region $R_\tau(x)$ to a reported output, such as a (possibly empty) set of labels—with abstention represented by \emptyset —or a single committed label. The deployed predictor is written as

$$\hat{C}_\pi(x) := \pi(R_\tau(x)).$$

The standard split conformal predictor corresponds to the set inclusion policy (Romano et al., 2019; Barber et al., 2021)

$$\pi_{\text{SI}}(r) := \{y \in \mathcal{Y} : r_y = 1\},$$

yielding

$$\hat{C}_{\pi_{\text{SI}}}(x) = \{y \in \mathcal{Y} : s(x, y) \leq \tau_y\},$$

with $\tau_y \equiv \tau$ in the pooled case.

The motivation for introducing policies is to separate calibration from action. Calibration fixes thresholds and therefore a finite set of region outcomes; deployment then chooses how to act on those outcomes. Writing $\hat{C}_\pi(x) = \pi(R_\tau(x))$ lets us swap or optimize decision rules for operational objectives (commit/defer/reject) without rewriting the calibration step, and it provides a common language for auditing and comparing policies.

As an example beyond set inclusion, consider a region-triggered commit policy. In the binary case $\mathcal{Y} = \{0, 1\}$, let $A \subseteq \{0, 1\}^2$ and $a \in \{0, 1\}$, and define

$$\pi_{A \rightarrow a}(r) = \begin{cases} \{a\}, & r \in A, \\ \emptyset, & r \notin A. \end{cases}$$

In words, the policy commits to action a only when the realized conformal region belongs to the pre-specified trigger set A ; otherwise it abstains. Thus A acts as an explicit commitment gate on the fixed calibrated region partition.

Figure 3 visualizes several other deployment policies acting as deterministic projections on a fixed region structure.

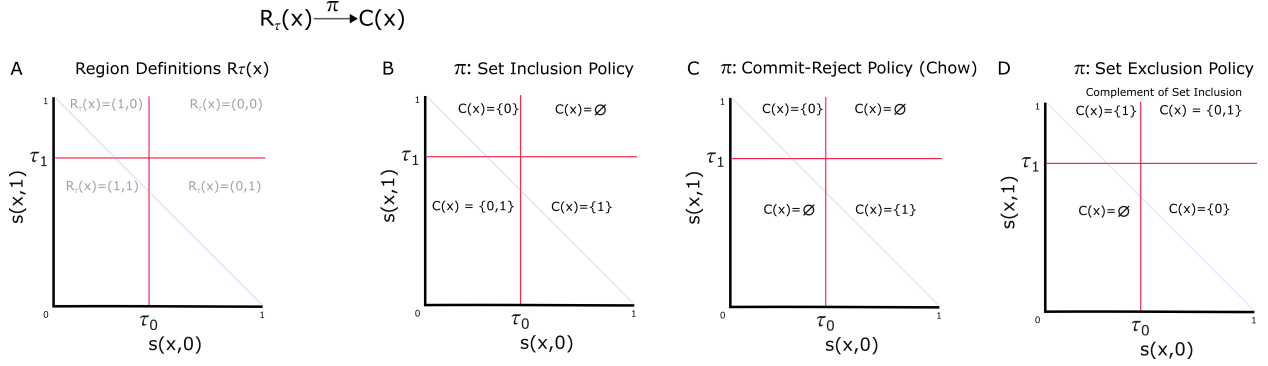


Figure 3: Deployment policies as projections on a fixed region structure. Panel A shows the region partition $R_\tau(x)$. Panels B–D apply different region-based deployment policies π to the same regions and data support, yielding reported outputs $\hat{C}_\pi(x) = \pi(R_\tau(x))$. Differences between panels arise solely from the choice of policy.

2.4 Auditing primitives: region–label tables and policy projections

Conditional on \mathcal{D}_{cal} , the deployed rule is fixed, and the primitive observable for auditing is the pair $(R_{\tau(\theta)}(X), Y)$ on an exchangeable labeled split. Two representations are useful: the full region–label table, and KPI indicators obtained as its projections. Here $\theta \in \Theta$ denotes a calibration setting that determines thresholds $\tau(\theta)$ and hence the region map $R_{\tau(\theta)}$.

(A) Region–label joint table. Define the calibration-conditional joint probabilities

$$p_{r,y}(\theta) := \mathbb{P}(R_{\tau(\theta)}(X) = r, Y = y \mid \mathcal{D}_{\text{cal}}), \quad (r, y) \in \mathcal{R} \times \mathcal{Y}.$$

These are fixed (but unknown) constants for the deployed rule. The audit set is used to estimate them via the counts

$$K_{r,y}^{\text{audit}}(\theta) := \sum_{i=1}^{n_{\text{audit}}} \mathbf{1}\{R_{\tau(\theta)}(X_i^a) = r, Y_i^a = y\}, \quad \hat{p}_{r,y}^{\text{audit}}(\theta) := \frac{K_{r,y}^{\text{audit}}(\theta)}{n_{\text{audit}}}.$$

Note that the region map $R_{\tau(\theta)}$ is fixed from \mathcal{D}_{cal} , while the counts $K_{r,y}^{\text{audit}}(\theta)$ are computed on $\mathcal{D}_{\text{audit}}$ only. Because $R_{\tau(\theta)}$ is a finite partition of score space, the region–label events $(R_{\tau(\theta)}(X) = r, Y = y)$ form a finite partition of the sample space. Consequently, for every θ ,

$$\sum_{r \in \mathcal{R}} \sum_{y \in \mathcal{Y}} p_{r,y}(\theta) = 1, \quad \sum_{r \in \mathcal{R}} \sum_{y \in \mathcal{Y}} \hat{p}_{r,y}^{\text{audit}}(\theta) = 1.$$

Moreover, the label marginals are fixed by the deployment data-generating process:

$$\sum_{r \in \mathcal{R}} p_{r,y}(\theta) = \mathbb{P}(Y = y \mid \mathcal{D}_{\text{cal}}), \quad \sum_{r \in \mathcal{R}} \hat{p}_{r,y}^{\text{audit}}(\theta) = \hat{\mathbb{P}}^{\text{audit}}(Y = y),$$

so varying θ reallocates mass across regions within each label. These conservation laws are the basic source of geometric coupling and explain why sweeping θ produces a constrained set of rate vectors rather than filling an ambient volume.

(B) Policy-specific indicators. Fix a deployment policy π . Any operational quantity of interest can be written as a Bernoulli indicator

$$I_\ell := g_\ell(R_{\tau(\theta)}(X), Y; \pi) \in \{0, 1\}, \quad p_\ell(\theta) := \mathbb{P}(I_\ell = 1 \mid \mathcal{D}_{\text{cal}}).$$

These operational targets are auditable event rates that summarize deployment behavior (e.g., abstention, decisiveness, decisive error exposure, or class-conditional region mass). For example, the abstention indicator

is $g_{\text{abs}}(r, y; \pi) = \mathbf{1}\{\pi(r) = \emptyset\}$, and a decisive error indicator is $g_{\text{err}}(r, y; \pi) = \mathbf{1}\{|\pi(r)| = 1, y \notin \pi(r)\}$. The corresponding audit count is

$$K_\ell^{\text{audit}}(\theta) := \sum_{i=1}^{n_{\text{audit}}} g_\ell(R_{\tau(\theta)}(X_i^a), Y_i^a; \pi), \quad \hat{p}_\ell^{\text{audit}}(\theta) := \frac{K_\ell^{\text{audit}}(\theta)}{n_{\text{audit}}}.$$

Projection identity. The two representations are linked by linearity: every linear KPI is obtained by summing selected region–label cells. On the audit sample,

$$K_\ell^{\text{audit}}(\theta) = \sum_{r \in \mathcal{R}} \sum_{y \in \mathcal{Y}} g_\ell(r, y; \pi) K_{r,y}^{\text{audit}}(\theta), \quad \hat{p}_\ell^{\text{audit}}(\theta) = \frac{K_\ell^{\text{audit}}(\theta)}{n_{\text{audit}}}. \quad (1)$$

Taking expectation yields the corresponding identity for latent rates:

$$p_\ell(\theta) = \sum_{r \in \mathcal{R}} \sum_{y \in \mathcal{Y}} g_\ell(r, y; \pi) p_{r,y}(\theta).$$

Thus the region–label table is a reusable sufficient audit summary: audit it once, then compute policy-level KPIs by projection. The same structure extends to monotone transformations of linear KPIs (e.g., ratios or log-odds), since the region–label table remains the sufficient summary.

Worked example: coverage as a projection of the region–label table. Consider $\mathcal{Y} = \{0, 1\}$ and the set-inclusion policy π_{SI} . For fixed thresholds, each input falls into one of four regions $\mathcal{R} = \{r_{10}, r_{11}, r_{01}, r_{00}\}$, and the primitive auditing object is $(R_\tau(X), Y) \in \mathcal{R} \times \mathcal{Y}$. The corresponding region–label table is

$$P(\theta) = \begin{array}{c|ccc} & y = 0 & y = 1 & \hat{C}_{\pi_{\text{SI}}}(X) \\ \hline r_{10} = (1, 0) & \mathbf{p}_{10,0}(\theta) & p_{10,1}(\theta) & \{0\} \\ r_{11} = (1, 1) & \mathbf{p}_{11,0}(\theta) & \mathbf{p}_{11,1}(\theta) & \{0, 1\} \\ r_{01} = (0, 1) & p_{01,0}(\theta) & \mathbf{p}_{01,1}(\theta) & \{1\} \\ r_{00} = (0, 0) & p_{00,0}(\theta) & p_{00,1}(\theta) & \emptyset \end{array} \quad \text{with} \quad \sum_{r \in \mathcal{R}} \sum_{y \in \mathcal{Y}} p_{r,y}(\theta) = 1.$$

Under π_{SI} , the event $\{Y \in \hat{C}_{\pi_{\text{SI}}}(X)\}$ corresponds to the four bold-indicated cells $(r_{10}, 0)$, $(r_{11}, 0)$, $(r_{11}, 1)$, and $(r_{01}, 1)$, hence

$$p_{\text{cov}}(\theta) = p_{10,0}(\theta) + p_{11,0}(\theta) + p_{11,1}(\theta) + p_{01,1}(\theta) = 1 - (p_{10,1}(\theta) + p_{01,0}(\theta) + p_{00,0}(\theta) + p_{00,1}(\theta)).$$

Note that the calibration choices (α_0^*, α_1^*) determine the class-conditional miscoverage primitives—namely the joint rates $p_{10,1}(\theta) + p_{00,1}(\theta)$ for $Y = 1$ and $p_{01,0}(\theta) + p_{00,0}(\theta)$ for $Y = 0$ —while the decomposition of these totals into wrong-singleton errors versus abstentions (including the overall empty-set rate $p_{00,0}(\theta) + p_{00,1}(\theta)$) is dictated by the deployment distribution. The above example makes explicit both (i) the projection form (coverage is a sum of cells) and (ii) the conservation constraint: once thresholds are fixed, coverage is determined by how mass is redistributed across regions.

The same “sum selected cells” structure applies to abstention/deferral, decisiveness, and decisive error exposure under any fixed policy. This is the sense in which operational quantities become first-class: it yields a single auditable summary from which many KPIs can be computed (and later renegotiated) by projection, while making the conservation constraints that drive trade-offs explicit.

3 Operational quantities as first-class objects

Deployment behavior is summarized by operational rates induced by a calibrated threshold geometry together with a fixed deployment policy π . Consistent with Section 2, we keep three layers distinct: (i) **geometry**, given by thresholds and the induced region map $R_\tau(\theta)$; (ii) **policy**, given by a deterministic projection $\pi : \mathcal{R} \rightarrow 2^{\mathcal{Y}}$; and (iii) **rates**, which quantify how often auditable region–label events occur under deployment.

The goal of this section is to make operational quantities *first-class*: to specify which rate statements are certifiable, which data split is required, and how trade-offs are explored without committing to a scalar objective. Our perspective is explicitly predictive: we seek conservative, distribution-free statements about future realized operational behavior over finite windows, conditional on the one-time calibration draw. The intended output is an auditable trade-off map $\theta \mapsto \mathbf{r}(\theta)$ linking calibration choices to operational profiles, together with an efficiency boundary. Here $\theta \in \Theta$ denotes a calibration setting, i.e., an index for the deployed thresholds $\tau(\theta)$ and induced region map $R_{\tau(\theta)}$.

3.1 Calibrate–and–Audit

Beyond marginal coverage, distribution-free finite-sample statements require an independent audit split (Bian & Barber, 2023; Gibbs et al., 2025). Coverage is special because its split-conformal guarantee is rank-based. For general region–label rates, reusing \mathcal{D}_{cal} couples region–label indicators to the random threshold and breaks the exchangeable Bernoulli model (Geisser, 1993; Casella & Berger, 2002) needed for exact predictive envelopes; therefore certified envelopes require an independent $\mathcal{D}_{\text{audit}}$ (Appendix D).

Using the audit split defined in Section 2, we keep thresholds (and thus $R_{\tau(\theta)}$) fixed from \mathcal{D}_{cal} and compute all operational rate estimates and predictive envelopes on $\mathcal{D}_{\text{audit}}$ only. As with the train/calibrate separation, once the rule depends on data, certification of downstream behavior requires fresh exchangeable evaluation data.

When a separate $\mathcal{D}_{\text{audit}}$ cannot be afforded, we provide a conservative procedure that aims to decouple threshold selection from rate estimation by evaluating each calibration point under a leave-one-out (LOO) proxy threshold that does not use that point. This proxy is intended for feasibility exploration rather than certification. In simulations, this procedure tracks the certified two-split reference closely; see Appendix D.

3.2 Certified predictive envelopes for future windows

Section 2 defines the auditable primitive: the joint process $(R_{\tau(\theta)}(X), Y)$ under fixed thresholds, together with KPI indicators obtained as linear projections of the corresponding region–label table (with coverage as a worked example). Under Calibrate–and–Audit, conditional on \mathcal{D}_{cal} the deployed rule (hence $R_{\tau(\theta)}$ and π) is fixed, and the audit points are exchangeable with future deployment points. Therefore, for any fixed indicator I_ℓ ,

$$K_\ell^{\text{audit}}(\theta) \mid \mathcal{D}_{\text{cal}} \sim \text{Binomial}(n_{\text{audit}}, p_\ell(\theta)),$$

and for a future operational window of size m with draws (X'_j, Y'_j) , the future realized count

$$K_\ell^m(\theta) := \sum_{j=1}^m g_\ell(R_{\tau(\theta)}(X'_j), Y'_j; \pi) \mid \mathcal{D}_{\text{cal}} \sim \text{Binomial}(m, p_\ell(\theta)).$$

These conditional Binomial laws (Johnson et al., 1997) induce distribution-free finite-sample predictive envelopes for $K_\ell^m(\theta)$, and hence for the realized window rate $\widehat{R}_{\ell, m} = K_\ell^m(\theta)/m$, based on the audit count $K_\ell^{\text{audit}}(\theta)$ observed on $\mathcal{D}_{\text{audit}}$.

The Beta–Binomial form is not a prior assumption on $p_\ell(\theta)$. It is a closed-form expression for the predictive distribution of $K_\ell^m(\theta)$ induced by the two-stage design: conditional on \mathcal{D}_{cal} , the audit indicators and future-window indicators are i.i.d. Bernoulli trials with a common (unknown) success probability $p_\ell(\theta)$. Observing the audit count $K_\ell^{\text{audit}}(\theta)$ therefore determines exact finite-sample predictive tails for $K_\ell^m(\theta)$ under exchangeability, which can be written in Beta–Binomial form.

As a conservative alternative, the same audit rate $\widehat{p}_\ell^{\text{audit}}(\theta)$ admits Hoeffding-type deviation inequalities (Hoeffding, 1963) for the latent rate $p_\ell(\theta)$. These yield worst-case planning envelopes for future window rates; we record them in Appendix D.

3.3 Rate vectors, attainable operational sets, and Pareto filtering

Certified envelopes (Section 3.2) apply to any fixed region–label event rate at any fixed calibration setting, and to any linear projection thereof. Deployment planning is comparative: stakeholders want to understand how operational behavior varies across calibration settings, which combinations of rates are feasible for a given scoring model and coverage semantics, and where structural bottlenecks lie. This motivates treating the *rate vector* (Miettinen, 1999) as the decision interface.

Let Θ denote a family of calibration settings (e.g., an α -grid or a class-conditional threshold family), and write $R_{\tau(\theta)}$ for the induced region map at setting θ . Fix a deployment policy π and a list of L auditable KPIs, each represented by an indicator $I_\ell = g_\ell(R_{\tau(\theta)}(X), Y; \pi)$. Define the calibration-conditional rate vector

$$\mathbf{r}(\theta) = (r_1(\theta), \dots, r_L(\theta)), \quad r_\ell(\theta) := \mathbb{P}(I_\ell = 1 \mid \mathcal{D}_{\text{cal}}).$$

Each coordinate is obtained by projection from the same audited region–label table via (1).

Attainable operational set and visualization. Sweeping θ traces the set of achievable operational profiles under the fixed policy π ,

$$\mathcal{V}(\Theta; \pi) := \{\mathbf{r}(\theta) : \theta \in \Theta\} \subset \mathbb{R}^L.$$

Because the region–label table obeys conservation constraints (sum-to-one and fixed label marginals), $\mathcal{V}(\Theta; \pi)$ is typically a constrained set: changing θ reallocates probability mass across regions and thus across KPIs, rather than tuning rates independently. Trade-off plots (e.g., Figure 1) display selected coordinates of $\hat{\mathbf{r}}^{\text{audit}}(\theta)$, optionally annotated with finite-window predictive envelopes computed from the projected audit counts.

Orientation and Pareto filtering (no cost model). To summarize negotiation-relevant regimes without committing to a scalar objective, we apply an *oriented* Pareto filter. Concretely, the analyst chooses, for each displayed KPI, whether it is desirable to be large or small (e.g., lower decisive error exposure is better; higher purity is better). This is an *orientation choice*, not a pricing model. Formally, fix an orientation vector $s \in \{-1, +1\}^L$ and compare points using $s \odot \mathbf{r}(\theta)$. A setting θ is *nondominated* if there is no θ' such that

$$s_\ell r_\ell(\theta') \geq s_\ell r_\ell(\theta) \text{ for all } \ell, \quad \text{and} \quad s_{\ell_0} r_{\ell_0}(\theta') > s_{\ell_0} r_{\ell_0}(\theta) \text{ for some } \ell_0.$$

The nondominated set is the *negotiation front*: any later decision rule that imposes hard constraints or introduces scalar weights must select an operating point on (or near) this front.

The resulting trade-off map answers a planning question: within the permissible calibration family Θ , what operational behaviors are attainable under the fixed policy π , and which of those behaviors survive as negotiation-relevant regimes? Predictive envelopes then attach finite-window uncertainty to the frontier points, supporting robust regime selection under operational constraints, or can be included to shape the pareto frontier directly.

3.4 SSBC as a calibration navigation coordinate

A trade-off map is most useful in practice when it admits a user-facing means of navigation tied to an agreed-upon semantic constraint. In this work we use coverage as that semantic anchor. Coverage is special among the KPIs considered above: under exchangeability, split conformal admits an exact finite-sample rank/Beta characterization of the *calibration-conditional* coverage (Marques, 2025). SSBC inverts this law to translate a semantic request (α^*, δ) into a concrete discrete choice on the conformal calibration grid (Appendices B and C).

Split conformal calibration selects thresholds on a finite grid of order statistics; equivalently, it can be indexed by the discrete miscoverage level $\alpha_{\text{grid}} = u/(n_{\text{cal}} + 1)$ with $u \in \{1, \dots, n_{\text{cal}}\}$ (or by the equivalent order-statistic index $k = n_{\text{cal}} + 1 - u$; see Section 2.2). SSBC maps (α^*, δ) to a single admissible index $u^*(\alpha^*, \delta)$ by selecting the least conservative grid point whose induced calibration-conditional coverage satisfies the

PAC-style tail requirement

$$\mathbb{P}_{\mathcal{D}_{\text{cal}}}\left(\mathbb{P}(Y \in \hat{C}(X) \mid \mathcal{D}_{\text{cal}}) \geq 1 - \alpha^*\right) \geq 1 - \delta.$$

Concretely, SSBC inverts the exact rank/Beta law and returns the boundary grid point that satisfies the δ -tail constraint with minimal conservatism.

This reduction is important for the geometry studied in Section 4: although a user specifies two parameters (α^*, δ) , SSBC returns a single discrete index u^* , hence a single threshold choice, Appendix C. That choice fixes the region map $R_{\tau(\theta)}$ and therefore fixes all KPIs in $\mathbf{r}(\theta)$.

In pooled split conformal there is one such index, yielding a one-parameter navigation along the conformal grid. In class-conditional calibration, SSBC is applied separately within each class. In the binary case this yields two indices

$$(u_0^*, u_1^*) = (u^*(\alpha_0^*, \delta_0), u^*(\alpha_1^*, \delta_1)),$$

which determine (τ_0, τ_1) and hence the calibration setting θ . Thus, while the user-facing specification appears four-dimensional $(\alpha_0^*, \delta_0, \alpha_1^*, \delta_1)$, SSBC collapses it to a two-dimensional navigation coordinate on the calibration grid.

Implication for attainable sets. Because θ is determined by these discrete indices, the calibration family Θ admits a low-dimensional parameterization (one-dimensional in the pooled case, two-dimensional in the binary Mondrian case) even before accounting for the conservation constraints in the region-label table. Section 4 then makes the resulting coupling explicit in the probability-normalized binary setting and explains the sharp regime boundaries observed when sweeping these navigation indices.

4 Consequences of a fixed conformal partition in the binary case

Fix a trained scoring function and a realized calibration draw. Calibration selects thresholds τ and therefore a fixed region process $R_{\tau}(X)$ (Section 2.3). All deployment-facing quantities in this paper are functionals of the joint region-label structure $(R_{\tau}(X), Y)$ (Section 3). In the binary case, treating the conformal interface as the object of planning has three concrete consequences: (i) *feasibility is coupled*—varying τ reallocates probability mass across finitely many region types rather than tuning rates independently; (ii) *posteriors are piecewise-constant*—any region-measurable policy acts only through within-region label composition; and (iii) *distribution-free is not cost-agnostic*—once actions are wired to regions, coherence with a cost or utility model imposes compatibility constraints that depend on the region-label table (Appendix F). We make these points explicit under probability-normalized scores.

4.1 Binary conformal geometry and regime boundaries

Let $\mathcal{Y} = \{0, 1\}$ and fix class-conditional thresholds $\tau = (\tau_0, \tau_1)$. The deployed interface is the region label

$$R_{\tau}(x) := (\mathbf{1}\{s(x, 0) \leq \tau_0\}, \mathbf{1}\{s(x, 1) \leq \tau_1\}) \in \{0, 1\}^2,$$

with outcomes 10, 11, 01, 00 (singleton-0, hedge, singleton-1, abstention under π_{SI}).

Probability-normalized scores induce a regime boundary. For probability-normalized scores $s(x, y) = 1 - P(y \mid x)$ we have $s(x, 0) + s(x, 1) = 1$. Hence a point cannot satisfy both class thresholds unless $\tau_0 + \tau_1 \geq 1$, and it cannot violate both unless $\tau_0 + \tau_1 \leq 1$. Consequently:

- **Hedging regime** ($\tau_0 + \tau_1 > 1$): 11 may occur and 00 cannot (singletons + hedges; no abstention).
- **Rejection regime** ($\tau_0 + \tau_1 < 1$): 00 may occur and 11 cannot (singletons + abstention; no hedges).
- **Boundary** ($\tau_0 + \tau_1 = 1$): only 10 and 01 occur; under π_{SI} outputs are always singletons.

Crossing $\tau_0 + \tau_1 = 1$ therefore changes which outcome types can appear. This is a deterministic constraint induced by the score normalization, not an estimation artifact. Note that when $\tau_0 = \tau_1 = 1/2$, the associated classification rule is the argmax rule and coverage equals the classifier’s accuracy.

Cross-threshold coupling within regimes. Within the hedging regime ($\tau_0 + \tau_1 > 1$), the diagonal support is partitioned into three contiguous intervals. Parameterize by $u = s(x, 0)$ (so $s(x, 1) = 1 - u$):

$$u \in [0, 1 - \tau_1) \Rightarrow R_\tau(x) = 10, \quad u \in [1 - \tau_1, \tau_0] \Rightarrow R_\tau(x) = 11, \quad u \in (\tau_0, 1] \Rightarrow R_\tau(x) = 01.$$

Thus region boundaries are governed by *opposing* thresholds: changing τ_1 moves the boundary that controls the mass of 10, while changing τ_0 moves the boundary that controls the mass of 01. Thresholds therefore act as mass-reallocation boundaries, not independent per-class knobs.

Sweeping calibration settings moves τ and reallocates mass across regions. When score support is low-dimensional, small changes in τ can trigger support discontinuities, and within regimes operational coordinates are coupled. Under probability-normalized scores, swapping (τ_0, τ_1) exchanges the roles of regions 11 and 00. If the deployment policy treats hedging and abstention identically, then this swap does not change action-level behavior, even though set-inclusion coverage changes.

4.2 Region-label tables, piecewise-constant posteriors, and coherent action

Fix τ and treat the region label $R_\tau(X) \in \{0, 1\}^2$ as the only deployed observable. The joint region-label probabilities

$$p_{r,y} := \mathbb{P}(R_\tau(X) = r, Y = y \mid \mathcal{D}_{\text{cal}}), \quad r \in \{0, 1\}^2, \quad y \in \{0, 1\},$$

fully characterize the information available to any region-measurable policy. Write $p_r := p_{r,0} + p_{r,1}$ for region mass. Because the interface takes finitely many values, the region-conditioned label composition is constant within each region; downstream evaluation and decision-making therefore reduce to functions of $(p_{r,0}, p_{r,1})$, aggregated across regions using the same table $\{p_{r,y}\}$.

Definition (cost-coherence for region-based action). Let \mathcal{A} be an action set and let $L(a, y)$ be the cost of taking action $a \in \mathcal{A}$ when $Y = y$. A region-based policy $\tilde{\pi} : \{0, 1\}^2 \rightarrow \mathcal{A}$ induces calibration-conditional expected cost

$$\mathcal{R}(\tilde{\pi}) := \sum_{r \in \{0, 1\}^2} \sum_{y \in \{0, 1\}} L(\tilde{\pi}(r), y) p_{r,y}.$$

We say $\tilde{\pi}$ is *cost-coherent* for the deployed interface if, for every region with $p_r > 0$, it minimizes conditional risk within that region:

$$\tilde{\pi}(r) \in \arg \min_{a \in \mathcal{A}} \frac{\sum_{y \in \{0, 1\}} L(a, y) p_{r,y}}{p_r} \quad \text{for all } r \text{ with } p_r > 0.$$

Because $\mathcal{R}(\tilde{\pi})$ separates across regions for unconstrained region-based policies, this local condition is equivalent to global optimality (ties arbitrary). We use the local form to state per-region compatibility conditions.

4.3 Conformal partitions are not cost-agnostic under coherent action

Cost-coherence makes a simple point operational: once a conformal partition is deployed, a downstream convention is rational only relative to the information carried by the region label and the costs of available actions. In particular, even if a region is labeled as a singleton under π_{SI} , coherence is determined by the region-label composition $(p_{r,0}, p_{r,1})$, not by the set label itself.

Reject-option example (Chow-style abstention). Following Chow (1970), consider actions $\mathcal{A} = \{0, 1, \text{rej}\}$ with false positive cost $c_{10} > 0$, false negative cost $c_{01} > 0$, rejection cost $c_{\text{rej}} \geq 0$, and zero cost for correct commitments. For each region r , define $p_r := p_{r,0} + p_{r,1}$. Cost-coherence is decided by comparing the three region-level alternatives:

$$\begin{aligned} \text{choose } 0 : & \quad p_{r,1}c_{01} \leq p_{r,0}c_{10} \quad \text{and} \quad p_{r,1}c_{01} \leq p_r c_{\text{rej}}, \\ \text{choose } 1 : & \quad p_{r,0}c_{10} \leq p_{r,1}c_{01} \quad \text{and} \quad p_{r,0}c_{10} \leq p_r c_{\text{rej}}, \\ \text{choose } \text{rej} : & \quad p_r c_{\text{rej}} \leq p_{r,1}c_{01} \quad \text{and} \quad p_r c_{\text{rej}} \leq p_{r,0}c_{10}. \end{aligned}$$

Thus, for a fixed convention, coherence means its prescribed action satisfies the corresponding inequalities in every region (ties allowed). For example, if the policy commits to class 0 in region 10 (singleton output $\{0\}$ under π_{SI}), then coherence requires $p_{10,1}c_{01} \leq p_{10,0}c_{10}$ and $p_{10,1}c_{01} \leq (p_{10,0} + p_{10,1})c_{\text{rej}}$. This also shows why the hard-wired convention “commit on singleton outputs; defer otherwise” is cost-coherent only if, in each singleton region with $p_r > 0$, the forced commitment has lower expected cost than both rejection and the opposite commitment: a region can be labeled by a singleton set under π_{SI} yet still favor rejection (or even the opposite commitment) for plausible cost ratios. More generally, coherence of any fixed (interface, convention) pair can be expressed as explicit inequalities in the region-label table $\{p_{r,y}\}$ and cost ratios such as $(c_{\text{rej}}/c_{01}, c_{\text{rej}}/c_{10})$; see Appendix F. That appendix also gives an inverse view: for a fixed convention, characterize the set of cost ratios under which it is coherent.

5 Results: validation and deployment-facing planning

This section reports results aligned with the paper’s deployment-facing claims for a single deployed scoring model: the model is treated as fixed infrastructure and we vary only calibration settings (hence the induced region geometry). We focus on three questions: (i) SSBC coverage semantics under calibration randomness and finite deployment windows, (ii) predictive envelopes for deployment-facing operational rates beyond coverage, and (iii) scenario planning via trade-off maps with cost-coherence screening.

5.1 Numerical Simulations

This subsection validates two core claims: SSBC preserves the intended finite-window coverage semantics under calibration randomness, and Calibrate-and-Audit provides well-centered predictive envelopes for deployment-facing operational rates. Table 1 summarizes semantic coverage behavior, and Figure 4 compares envelope alignment between two-sample and LOO constructions.

5.1.1 Coverage: numerical realization of SSBC guarantees

This experiment instantiates the exact finite-sample laws underlying SSBC in the finite-window deployment regime, separating calibration randomness from deployment-window noise. Calibration nonconformity scores are drawn i.i.d. from a continuous, heavy-tailed reference distribution, chosen as the absolute Cauchy distribution $|t_{\nu=1}|$ to remain agnostic to model specifics.

For each calibration set size n_{cal} , split conformal selects a threshold via a discrete miscoverage index $u \in \{1, \dots, n_{\text{cal}}\}$ with

$$\alpha_{\text{grid}} = \frac{u}{n_{\text{cal}} + 1}, \quad k = n_{\text{cal}} + 1 - u, \quad \tau = S_{(k)}.$$

We compare three index-selection rules at target $(\alpha^*, \delta) = (0.10, 0.10)$: nominal split conformal, a DKWM correction (Massart, 1990; Dvoretzky et al., 1956), and SSBC, Appendix C. In the latter case, we distinguish between the infinite window and finite window cases that follow a Beta and Beta-Binomial law, respectively.

Table 1 shows representative calibration sizes (full grid in Appendix C). Nominal split conformal undercontrols calibration-conditional risk; DKWM enforces validity through strong conservatism. SSBC directly inverts the relevant finite-window law, yielding violation probabilities close to the target δ up to grid effects.

5.1.2 Operational rate envelopes: LOO versus two-sample reference

We next validate predictive envelopes for operational rates beyond coverage, where no distribution-free rank pivot exists. The goal is to compare the certified two-sample Calibrate-and-Audit construction to a single-sample LOO surrogate intended for feasibility exploration.

Synthetic probability model. We generate predicted probabilities and labels so the score geometry is controlled and interpretable. Each draw produces $Y \in \{0, 1\}$ with $\mathbb{P}(Y = 1) = p_{\text{class}}$, where $p_{\text{class}} \in \{0.10, 0.50\}$. Conditional on Y , we draw P_1 via

$$P_1 \mid Y = 1 \sim \text{Beta}(a, b), \quad P_1 \mid Y = 0 \sim \text{Beta}(2, 7),$$

Table 1: **Representative calibration-conditional coverage violation rates.** Target miscoverage $\alpha^* = 0.10$, confidence $\delta = 0.10$, and deployment window size $m_{\text{infer}} = 100$. We report three representative calibration sizes; the complete grid is in Table 7.

n_{cal}	Method	u	α_{grid}	Obs	BetaTheory	BBTheory	α_{cont}
100	None	10	0.0990	0.4075	0.4513	0.4071	–
100	SSBC	6	0.0594	0.0960	0.0576	0.0956	–
100	DKWM	1	0.0099	0.0004	0.0000	0.0004	–0.0224
200	None	20	0.0995	0.4130	0.4655	0.4124	–
200	SSBC	13	0.0647	0.0974	0.0320	0.0980	–
200	DKWM	2	0.0100	0.0000	0.0000	0.0000	+0.0135
500	None	50	0.0998	0.4153	0.4782	0.4153	–
500	SSBC	34	0.0679	0.0949	0.0049	0.0955	–
500	DKWM	22	0.0439	0.0097	0.0000	0.0096	+0.0453

with $(a, b) \in \{(4, 3), (9, 3)\}$, form $(P_0, P_1) = (1 - P_1, P_1)$, and use class-conditional scores $S_y := 1 - P_y$.

Two-sample reference and LOO surrogate. For each configuration, we draw independent datasets \mathcal{D}_1 and \mathcal{D}_2 of size $N = 500$. We calibrate on \mathcal{D}_1 (including SSBC-adjusted thresholds at $(\alpha, \delta) = (0.10, 0.10)$ in the finite-window regime), freeze the induced rule, and evaluate operational indicators on \mathcal{D}_2 , yielding exact Binomial/Beta–Binomial predictive envelopes. As a single-sample surrogate, we compute LOO operational indicators by evaluating each point under thresholds recomputed without that point, pool LOO counts, and map them to envelopes; optionally we widen intervals via controlled pessimization (Appendix D).

Figure 4 shows that LOO-based envelopes closely match the two-sample reference in both location and width across all four geometries, while inflation widens intervals without shifting centers. This supports using LOO as a practical proxy for planning when an explicit audit split is unavailable, while keeping certification tied to the two-sample design.

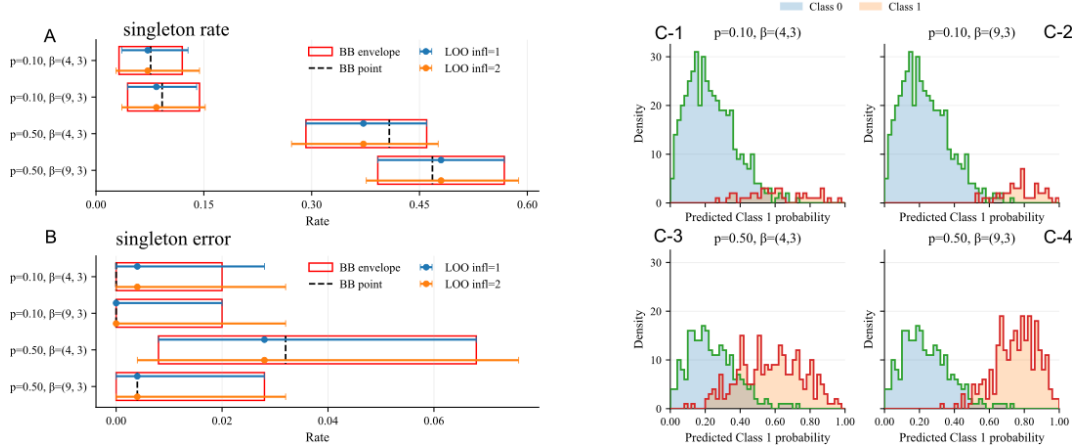


Figure 4: Operational rate envelopes and underlying score distributions. **(A)** Singleton rate and **(B)** singleton error for two class prevalences ($p_{\text{class}} = 0.10, 0.50$) and two class 1 generating distributions (Beta(4, 3) and Beta(9, 3)), with class 0 generated by Beta(2, 7). Red rectangles denote the two-sample Calibrate–and–Audit Beta–Binomial (BB) predictive envelope, and the dashed vertical line is the corresponding BB point estimate. Blue and orange markers with horizontal intervals show leave-one-out (LOO) envelopes computed from a single calibration dataset under two inflation levels (infl = 1, 2). **(C1–C4)** Histograms of the score geometry shown as predicted class 1 probability (equivalently, nonconformity to class 0) stratified by true class. These distributions make explicit how class prevalence and calibration geometry shape singleton mass and singleton error, and explain the regime-dependent asymmetry of the finite-sample envelopes.

These simulations support the calibration and envelope semantics used in the two real-data studies below.

5.2 Tox21: predictive envelopes under severe class imbalance

The Tox21 benchmark (Mayr et al., 2016; Huang et al., 2016) stress-tests the framework under severe class imbalance, where minority-class calibration counts can be well below 100 (Table 2). We evaluate (i) SSBC semantic coverage behavior under small class-conditional calibration sizes and (ii) finite-window operational envelopes in a practical setting. Table 3 summarizes aggregated semantic behavior; endpoint-level operational envelope comparisons appear in Table 4 and Appendix H.

Tasks and modeling infrastructure. Tox21 comprises twelve binary toxicity endpoints (NR and SR pathways). Each endpoint is treated as an independent binary classification problem. Molecules are represented using RDKit (Landrum, 2025) 2D descriptors augmented with Morgan fingerprints (Rogers & Hahn, 2010) (radius 2, 128 bits), and classification is performed using CatBoost (Prokhorenkova et al., 2018) with fixed hyperparameters. For each endpoint, data are split randomly into training (50%), calibration (25%), and test (25%), and results are averaged over 100 splits. Conformal calibration is class-conditional and we compare: (i) standard split conformal, (ii) DKWM correction, and (iii) SSBC, all at $(\alpha, \delta) = (0.10, 0.10)$.

Table 2: Tox21 dataset composition and effective class-conditional calibration sizes under the experimental protocol.

Endpoint	Total Samples	Positive Rate	Calib. Positives	Calib. Negatives
NR-AR	7265	4.3%	77	1739
NR-AR-LBD	6758	3.5%	59	1630
NR-AhR	6549	11.7%	192	1445
NR-Aromatase	5821	5.2%	75	1380
NR-ER	6193	12.8%	198	1350
NR-ER-LBD	6955	5.0%	87	1651
NR-PPAR- γ	6450	2.9%	46	1566
SR-ARE	5832	16.2%	235	1223
SR-ATAD5	7072	3.7%	66	1702
SR-HSE	6467	5.8%	93	1523
SR-MMP	5810	15.8%	229	1223
SR-p53	6774	6.2%	105	1587

5.2.1 Coverage semantics under small class-conditional calibration sizes

Table 3 aggregates empirical coverage, violation rates, and prediction-set statistics over all endpoints and splits. Nominal split conformal exhibits elevated violation probability in this conditional small- n regime. DKWM enforces validity through conservatism, inflating set sizes and reducing singleton frequency. SSBC substantially reduces violation probability while retaining more decisiveness than DKWM.

Table 3: Aggregated coverage and prediction-set statistics on Tox21. Results are averaged over twelve endpoints and 100 random splits. Violation rate is the empirical probability that coverage falls below the target level.

Method	Coverage	Violation Rate	Avg. Set Size	Singleton Rate
Standard Split Conformal	0.917	0.305	1.41	0.52
DKWM Correction	0.986	0.005	1.78	0.22
SSBC (proposed)	0.951	0.068	1.54	0.40

5.2.2 Operational envelopes as predictive summaries (LOO versus a two-sample reference)

With coverage risk fixed, we evaluate predictive envelopes for operational quantities over a finite deployment window. Operational KPIs are region-label indicators (Section 2.4); in the binary case, singleton mass, doublet mass, and wrong-singleton mass provide a compact KPI set tied directly to decisiveness and decisive error exposure.

Table 4: **SR-MMP endpoint.** Operational performance summary for the SR-MMP endpoint. All reported quantities are joint probabilities normalized by the total test-set size. Rows report the singleton and doublet joint event rates $P(Y = c, |S| = 1)$ and $P(Y = c, |S| = 2)$, together with the wrong-singleton rate $P(Y = c, |S| = 1, \hat{y} \neq Y)$, by true class. “point estimate \mathcal{D}_1 ” and “LOO 95% PI \mathcal{D}_1 ” denote leave-one-out point estimates and their beta–binomial predictive intervals computed on the calibration data. “Observed \mathcal{D}_2 ” reports empirical rates on an independent hold-out set. “BB 95% PI \mathcal{D}_2 ” gives the beta–binomial predictive intervals for the corresponding \mathcal{D}_2 quantities, accounting for calibration uncertainty and finite test size.

Operational quantity	Class	point estimate \mathcal{D}_1	LOO 95% PI \mathcal{D}_1	Observed \mathcal{D}_2	BB 95% PI \mathcal{D}_2
Singleton rate	Class 0	0.662	[0.604, 0.718]	0.651	[0.615, 0.686]
	Class 1	0.130	[0.092, 0.173]	0.117	[0.094, 0.142]
Doublet rate	Class 0	0.163	[0.121, 0.211]	0.201	[0.172, 0.231]
	Class 1	0.045	[0.023, 0.074]	0.031	[0.020, 0.046]
Wrong-singleton rate	Class 0	0.073	[0.044, 0.107]	0.070	[0.052, 0.090]
	Class 1	0.012	[0.002, 0.030]	0.011	[0.005, 0.020]

We compare the two-sample Calibrate–and–Audit reference to the single-sample LOO surrogate (Appendix D). Table 4 provides a representative endpoint-level breakdown; an additional endpoint is reported in Appendix H (Table 8). LOO point estimates track two-sample observed rates and intervals are comparable (often slightly wider), consistent with LOO primarily affecting predictive dispersion rather than centering.

5.3 R3: scenario planning on aqueous solubility

We now demonstrate the planning use-case: exploring attainable deployment-facing trade-offs across calibration settings without committing to a single scalar objective. We focus on aqueous solubility in drug development using AquaSolDB (Sorkun et al., 2019). The predictive model is treated as fixed infrastructure; variation is entirely through the calibration layer (SSBC), the induced conformal partition, and the downstream interpretation of the resulting finite interface.

Methodological setup (documented in Appendix I). This experiment is designed to separate (i) generalization across chemical space from (ii) exchangeable evaluation for conformal and finite-window forecasting. We therefore use scaffold-isolated training, followed by an exchangeable calibration/test design on the held-out scaffold-disjoint pool (Appendix I, dataset/partitioning/model details). Although the base classifier is trained on a three-class discretization of $\log S$ (Insoluble / Moderate / Soluble), deployment-facing planning is posed as a binary campaign objective by merging Moderate and Soluble into a single Soluble class and calibrating prediction sets in $\{\text{Ins}, \text{Sol}\}$ (Appendix I, calibration and operationalization).

Operational planning additionally requires a scenario definition: rather than assuming the full calibration pool matches deployment, we restore exchangeability by design for a specified deployment scenario by restricting calibration to a chemically defined subpopulation (Appendix I, Section I.8). In this study the focal scenario is a lipophilic deployment regime $\{\text{MolLogP} > 3.5\}$, and SSBC thresholds (and all envelopes derived from them) are computed using the restricted calibration sample.

Operating points and audited outcomes. For each SSBC setting, calibration fixes thresholds and therefore a discrete binary conformal interface (singleton- $\{\text{Sol}\}$, singleton- $\{\text{Ins}\}$, or doublet $\{\text{Sol}, \text{Ins}\}$). We interpret singletons as decisive commitments and the doublet as deferral, and summarize each setting by the joint outcome allocation $P(Y = y, C = c)$ over $y \in \{\text{Sol}, \text{Ins}\}$ and $c \in \{\{\text{Sol}\}, \{\text{Ins}\}, \{\text{Sol}, \text{Ins}\}\}$ (Table 5).

Table 5: Operational outcome categories induced by binary prediction sets.

True label Y	$C(X) = \{\text{Sol}\}$	$C(X) = \{\text{Ins}\}$	$C(X) = \{\text{Ins}, \text{Sol}\}$
Sol	TP (correct Sol singleton)	FN (loss)	HP (hedged Sol)
Ins	FP (waste)	TN (correct Ins singleton)	HN (hedged Ins)

Joint rates are the auditable primitive: they form a complete mass allocation over the set-label outcome space and map directly to expected finite-window counts (e.g., $m \times P(Y = y, C = c)$ for a window of size m). Because the conformal grid is discrete and behavior is determined by threshold geometry, many nominally distinct $(\alpha_0, \delta_0, \alpha_1, \delta_1)$ settings collapse to identical realized interfaces and joint allocations; we therefore deduplicate settings and retain the least conservative representative among equivalence classes (Appendix I).

Trade-off map and cost-coherence analysis. Figure 5 embodies the main results of this study. The left panel plots the attainable set in a KPI plane spanned by two soluble-class joint rates: irreversible exclusion $P(Y = \text{Sol}, C = \{\text{Ins}\})$ and deferral burden $P(Y = \text{Sol}, C = \{\text{Sol}, \text{Ins}\})$, with color encoding the decisive-correct soluble mass $P(Y = \text{Sol}, C = \{\text{Sol}\})$. We highlight nondominated regimes using an orientation-only Pareto filter over these three soluble-class quantities, yielding a shortlist of negotiation-relevant operating regimes.

Because a deployed conformal predictor is an information interface, we also screen regimes for rationality of a fixed downstream wiring given only the conformal output (Section 4.3). The right panel summarizes cost-coherence of the action policy $\{\text{Sol}\} \rightarrow \text{Sol}$, $\{\text{Ins}\} \rightarrow \text{Ins}$, $\{\text{Sol}, \text{Ins}\} \rightarrow \text{rej}$ over relative cost ratios $\lambda = c_{01}/c_{10}$ and $\rho = c_{\text{rej}}/c_{10}$. This analysis indicates that points on the Pareto front are cost-coherent for only a limited range of cost ratios: if the cost of irreversible exclusion is too high relative to the cost of deferral, or the cost of deferral is too high relative to the cost of irreversible exclusion, then the action policy yields decisions that yield higher expected costs than the alternative actions in those regions.

Additional results and documentation (appendix). Appendix I provides the supporting methodological record and supplementary empirical summaries used to interpret Figure 5: (i) dataset and label construction, scaffold-isolated partitioning, features, and model protocol; (ii) scenario-conditional (tribe-based) calibration restriction and its interpretation; and (iii) diagnostics on the functional roles of $(\alpha_0, \delta_0, \alpha_1, \delta_1)$ along the Pareto front, together with a discussion of how α - and δ -variation act as coarse versus fine adjustments under finite-sample SSBC geometry (Appendix I, Sections I.9–I.10).

6 Discussion

This work uses conformal prediction as deployed decision infrastructure, where the object of interest is not a one-off marginal guarantee but the realized behavior of a fixed rule over a finite operational window. In that regime, the key quantities are operational rate vectors—commitment, abstention, and error exposure—that govern downstream workload and harm. The central message is that coverage is special: because it depends only on the rank of the future true-label score among calibration scores (David & Nagaraja, 2003), its calibration-conditional variability admits an exact, distribution-free finite-sample characterization. Most other deployment KPIs do not share this pivot structure; they depend on multi-score geometry and threshold interactions, so validity must be handled by explicit auditing and uncertainty propagation.

The first contribution, Small-Sample Beta Correction (SSBC), addresses a practical mismatch between a user’s requested coverage level and what nominal split conformal delivers when the calibration set is small. The simulations show that nominal grid selection can yield large calibration-conditional violation probabilities, driven purely by calibration randomness, even when exchangeability holds. SSBC restores an operational semantics by selecting the calibration index through inversion of the exact Beta or Beta–Binomial laws, depending on whether one targets the long-run or finite-window coverage event. In contrast, DKWM-style corrections (Massart, 1990) achieve control primarily through conservatism, often pushing the system to overly abstain. SSBC therefore offers a useful middle ground: it is still distribution-free, but it allocates conservatism only where the finite-sample semantics demand it.

The second contribution, Calibrate-and-Audit, makes explicit a fact that is often implicit in practice: once calibrated, a conformal rule induces a finite partition of score space with a small set of region labels, and downstream systems inevitably map those region labels to actions. By estimating the region masses and region-label composition, the audit table marginalizes the calibration-induced geometry into a reusable empirical interface. This enables forward-looking predictive envelopes for operational rates over future

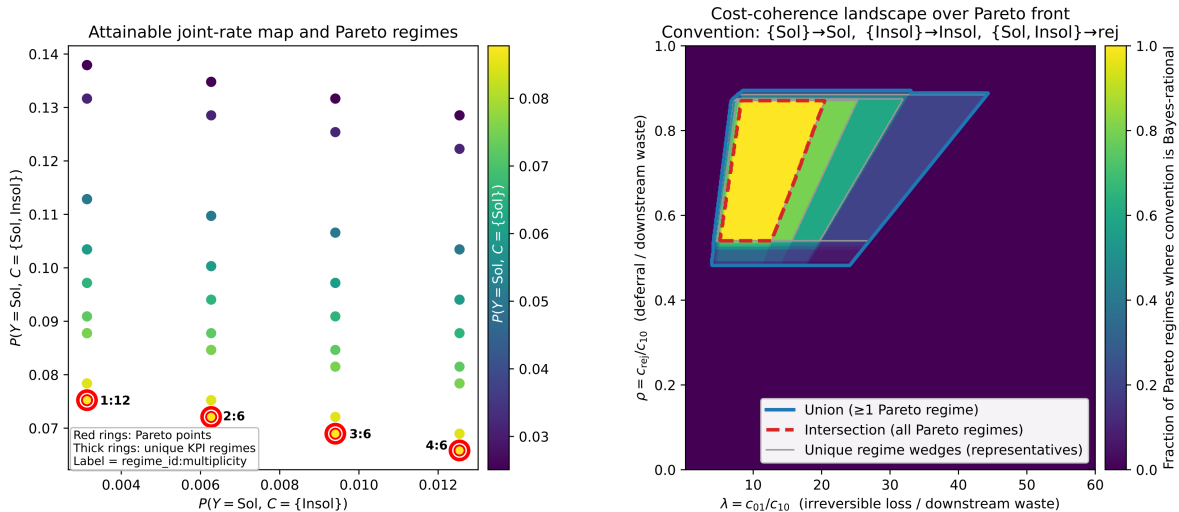


Figure 5: **Solubility scenario planning via conformal operating regimes and cost-coherence.** Left: attainable joint-rate map induced by sweeping SSBC calibration settings (after deduplication). Axes report joint rates on soluble compounds: irreversible exclusion $P(Y = \text{Sol}, C = \{\text{Insol}\})$ (x-axis) and deferral burden $P(Y = \text{Sol}, C = \{\text{Sol}, \text{Insol}\})$ (y-axis). Color encodes the joint decisive-correct rate $P(Y = \text{Sol}, C = \{\text{Sol}\})$. Red rings mark Pareto-optimal operating points; thick rings mark unique KPI regimes, labeled by `regime_id:multiplicity`. Right: cost-coherence landscape for the fixed downstream convention $\{\text{Sol}\} \rightarrow \text{Sol}$, $\{\text{Insol}\} \rightarrow \text{Insol}$, $\{\text{Sol}, \text{Insol}\} \rightarrow \text{rej}$, parameterized by cost ratios $\lambda = c_{01}/c_{10}$ (irreversible loss / downstream waste) and $\rho = c_{\text{rej}}/c_{10}$ (deferral / downstream waste). The heatmap shows the fraction of Pareto regimes for which this convention is cost-coherent given only the conformal output (via within-region label composition). Blue and red outlines give the union and intersection of feasible (λ, ρ) regions across the Pareto front; thin outlines show representative wedges for the unique KPI regimes.

windows, and supports scenario planning over attainable trade-offs across calibration settings. The results illustrate that operational fronts can be explored without retraining the base model, and that uncertainty in these fronts is quantifiable when one treats calibration as a one-time random event and deployment as finite-window sampling.

A key conceptual implication is the feasibility coupling induced by a fixed partition. Because the same conformal interface must serve multiple downstream objectives, not all combinations of commit and error exposure are simultaneously achievable by tuning a single scalar calibration parameter. The regime structure observed in trade-off curves is therefore not an artifact of a particular synthetic model; it follows from the constrained geometry of the induced regions. This perspective also clarifies when cost-aware operation is coherent. Action coherence depends on within-region label frequencies; if a region is label-mixed, forced commitment can be cost-incoherent across plausible cost ratios.

Several limitations delineate the scope of these guarantees. First, the distribution-free statements rely on exchangeability; dataset shift or model drift (Tibshirani et al., 2019; Fannjiang et al., 2022) breaks the exact finite-sample laws and must be handled by monitoring, re-calibration (Vovk, 2015; Barber et al., 2021), or domain-adaptive variants. Second, SSBC is tied to the discrete split-conformal grid; unavoidable granularity appears at small n_{cal} , and very strict (α^*, δ) targets may be unattainable without larger calibration sets. Third, the audit-based envelopes inherit variance from region sparsity; rare regions may require pooling, hierarchical smoothing, or targeted data collection. Finally, we focused on binary classification for clarity. Extending the action-coherence analysis to multi-class, structured outputs, or complex abstention policies is an important next step.

Overall, the paper argues for separating coverage guarantees from operational planning, i.e. what workload and harm rates a deployed conformal interface will induce. SSBC supplies the former, while Calibrate-and–

Audit supplies the latter. Together, they support a deployment workflow in which coverage is treated as a calibrated contract and the remaining KPIs are treated as audited, forecasted quantities with explicit, distribution-free finite-sample uncertainty.

7 Conclusion

We studied conformal prediction in the setting that matters for deployment: a single calibrated rule reused over finite operational windows. In this regime, coverage alone admits an exact, distribution-free calibration-conditional law, while other operational KPIs require explicit auditing.

SSBC provides a deterministic calibration-index selection rule that aligns a user’s coverage request with a PAC-style operational semantics under small calibration sets, including the finite-window case via the induced Beta-Binomial law. Calibrate-and-Audit complements this by turning the calibrated conformal predictor into a reusable region-label interface, enabling predictive envelopes for future commitment, abstention, and error-exposure rates and supporting scenario planning over attainable trade-offs.

Taken together, these tools move conformal prediction (Angelopoulos & Bates, 2023) from a single coverage guarantee toward a practical planning framework: coverage is treated as a contract with calibrated semantics, and the rest of the deployed behavior is forecasted and stress-tested with finite-sample uncertainty. Future work should focus on robust monitoring under shift, partition refinement to improve decision coherence, and extensions to richer output spaces and downstream policies.

A Appendix Outline & Notation

This appendix serves as a notation guide for the technical appendices that follow. The remaining material is organized as follows:

- **SSBC and coverage pivots:** derivations and calibration-conditional guarantees for grid selection, finite-sample behavior, and pivot-based uncertainty control.
- **Operational rates and LOO justification:** construction of deployment-facing rate envelopes, together with single-sample leave-one-out surrogates and their assumptions.
- **Geometry and binary partitions:** structural analysis for region definitions and indicator decompositions used in operational auditing.
- **Empirical case studies:** additional experimental details and results for Tox21 and Solubility.

The notation below is shared across split conformal calibration, the Small-Sample Beta Correction (SSBC), and finite-window prediction of operational rates. The analysis mixes three layers: (i) discrete split-conformal thresholding via order statistics on calibration scores; (ii) SSBC grid selection and calibration-conditional coverage semantics; and (iii) predictive envelopes for deployment-facing operational rates (Calibrate-and-Audit and a single-sample leave-one-out (LOO) surrogate). To avoid collisions, we reserve (k, u) exclusively for split conformal thresholding. Pooled LOO indicator counts use N_{loo} .

Table 6: Key notation used across calibration, SSBC, and operational analysis.

Symbol	Meaning	Scope / Remarks
<i>Data splits and window sizes</i>		
\mathcal{D}_{cal}	Calibration dataset	Exchangeable sample used to set conformal thresholds; size n_{cal} .
$\mathcal{D}_{\text{audit}}$	Audit / evaluation dataset	Exchangeable sample used to estimate region-label or event counts for operational envelopes.
n_{cal}	Calibration sample size	Number of points in \mathcal{D}_{cal} .
m	Future (deployment) window size	Number of future cases over which realized rates (and predictive envelopes) are defined.
<i>Split conformal thresholding and SSBC</i>		
$s(x, y)$	Nonconformity score function	Real-valued score for candidate label y at input x ; larger means “less conforming.”
$S_i := s(X_i, Y_i)$	True-label calibration scores	Scores computed on \mathcal{D}_{cal} ; exchangeable with the future score S_{n+1} .
$S_{(k)}$	k th order statistic of $\{S_i\}_{i=1}^{n_{\text{cal}}}$	Used to define the deployed split-conformal threshold τ .
k	Order-statistic index	Split conformal threshold index; $k \in \{1, \dots, n_{\text{cal}}\}$.
$u := n_{\text{cal}} + 1 - k$	Miscoverage grid index	Equivalent parametrization of the conformal grid; $u \in \{1, \dots, n_{\text{cal}}\}$.
$\alpha_{\text{grid}} := \frac{u}{n_{\text{cal}} + 1}$	Grid-aligned miscoverage level	Miscoverage induced by selecting index u on the discrete conformal grid.
$\tau := S_{(k)}$	Deployed conformal threshold	Fixed after calibration; determines the prediction-set map $C(\cdot)$.
α^*	Target (requested) miscoverage	User-facing miscoverage level prior to discretization / SSBC selection.
δ	Confidence (risk) parameter	Tail probability for calibration-conditional under-coverage events (PAC-style semantics).
$p_{\text{cov}}(\mathcal{D}_{\text{cal}})$	Calibration-conditional coverage probability	$p_{\text{cov}} := \mathbb{P}(Y \in C(X) \mid \mathcal{D}_{\text{cal}})$; random over calibration draws. Under exchangeability, $p_{\text{cov}} \sim \text{Beta}(k, u)$ for split conformal.
\widehat{C}_m	Finite-window empirical coverage	$\widehat{C}_m := \frac{1}{m} \sum_{j=1}^m \mathbf{1}\{Y'_j \in C(X'_j)\}$ over a future window of size m ; $m = \infty$ denotes the infinite-window (calibration-conditional) regime.
<i>Operational indicators, rates, and predictive envelopes</i>		
$C(X)$	Conformal prediction set	Set-valued output of the deployed rule at input X .
$g_\ell(\cdot)$	Operational event functional	Indicator map $g_\ell(C(X), Y) \in \{0, 1\}$ defining KPI/event ℓ (e.g., singleton, wrong-singleton, hedged-positive).
$I_{\ell, i}$	Operational indicator (deployed rule)	$I_{\ell, i} := g_\ell(C(X_i), Y_i)$ on an evaluation or deployment sample.
K_ℓ^m	Future event count over a window	$K_\ell^m := \sum_{j=1}^m I_{\ell, j}$; the object governed by Binomial/Beta–Binomial predictive laws.
$\hat{R}_\ell := \frac{1}{m} \sum_{j=1}^m I_{\ell, j}$	Realized operational rate over a window	Empirical rate $\hat{R}_\ell = K_\ell^m/m$ over a window of size m .
<i>Single-sample LOO surrogate (one dataset reuse)</i>		
$Z_{\ell, i}$	LOO operational indicator	$Z_{\ell, i} := g_\ell(C^{(-i)}(X_i), Y_i)$ where $C^{(-i)}$ is calibrated on $\mathcal{D}_{\text{cal}} \setminus \{(X_i, Y_i)\}$.
$N_{\text{loo}, \ell} := \sum_{i=1}^{n_{\text{cal}}} Z_{\ell, i}$	Pooled LOO indicator count	LOO “success” count used to form LOO-based estimates and envelopes for event ℓ ; distinct from conformal (k, u) .
$\hat{r}_{\text{loo}, \ell} := \frac{N_{\text{loo}, \ell}}{n_{\text{cal}}}$	Pooled LOO rate estimate	Convenience notation for the pooled LOO event frequency.
infl	Inflation factor (controlled pessimization)	Variance/width inflation used to hedge against dependence from single-sample reuse; implemented via $m_{\text{eff}} = m/\text{infl}$.

B Exact finite-sample law of calibration-conditional coverage

This appendix derives an exact finite-sample characterization of the *calibration-conditional coverage* of a fixed split conformal predictor under exchangeability. The key point is that coverage is a pure *rank* event: the future true-label score is compared to a calibration order statistic. This yields a distribution-free pivot and an exact Beta law for realized (calibration-conditional) coverage across calibration draws. This pivot is the input to SSBC (Appendix C).

B.1 Setup

Let $\mathcal{D}_{\text{cal}} = \{(X_i, Y_i)\}_{i=1}^n$ be exchangeable with a future test pair (X_{n+1}, Y_{n+1}) . Let $s(x, y)$ be a nonconformity score and define

$$S_i := s(X_i, Y_i), \quad i = 1, \dots, n, \quad \text{and} \quad S_{n+1} := s(X_{n+1}, Y_{n+1}).$$

Fix an index $k \in \{1, \dots, n\}$ and set

$$\tau := S_{(k)}, \quad u := n + 1 - k, \quad \alpha_{\text{grid}} = \frac{u}{n + 1}.$$

For the predictor calibrated on \mathcal{D}_{cal} , the *calibration-conditional coverage probability* is

$$p_{\text{cov}}(\mathcal{D}_{\text{cal}}) := \mathbb{P}(S_{n+1} \leq \tau \mid \mathcal{D}_{\text{cal}}).$$

This random variable varies across calibration draws but is fixed once calibration is completed.

B.2 Rank pivot

Assume for clarity that the score distribution is continuous so ties occur with probability zero (ties are addressed in Remark 1). Under exchangeability of $\{S_1, \dots, S_n, S_{n+1}\}$, the rank

$$R := \text{rank}(S_{n+1} \text{ among } S_1, \dots, S_n, S_{n+1})$$

is uniform on $\{1, \dots, n + 1\}$ (David & Nagaraja, 2003). Since $\tau = S_{(k)}$,

$$\{S_{n+1} \leq \tau\} \iff \{R \leq k\}.$$

Thus coverage is the conditional probability of a rank event.

B.3 Exact distribution: Beta law

A standard order-statistic identity implies that the conditional probability of the rank event equals the k th order statistic of $n + 1$ i.i.d. uniforms:

$$p_{\text{cov}}(\mathcal{D}_{\text{cal}}) \stackrel{d}{=} U_{(k)}, \quad U_{(k)} \sim \text{Beta}(k, u), \quad u = n + 1 - k,$$

where $U_{(k)}$ is the k th order statistic of $U_1, \dots, U_{n+1} \stackrel{\text{i.i.d.}}{\sim} \text{Unif}(0, 1)$ (David & Nagaraja, 2003). Equivalently, for any $t \in [0, 1]$,

$$\mathbb{P}(p_{\text{cov}}(\mathcal{D}_{\text{cal}}) \leq t) = I_t(k, u),$$

where $I_t(\cdot, \cdot)$ is the regularized incomplete Beta function. The law is distribution-free and depends only on (n, k) (equivalently (n, u)).

Remark 1 (Discrete scores and ties). If scores have atoms, ranks are not almost surely unique. Exact pivots can be recovered by randomized tie-breaking; deterministic left/right-continuous conventions yield conservative bounds. The non-interpolated order-statistic thresholding convention used in the main text preserves finite-sample validity.

Why coverage is special. Coverage depends only on the rank of the future true-label score relative to the calibration scores, hence admits an exact finite-sample distribution-free law. Most other operational KPIs depend on the joint geometry of multiple label scores and threshold interactions and therefore do not admit an analogous pivot (Appendix D).

C Small-Sample Beta Correction (SSBC)

SSBC is a deterministic index-selection rule for split conformal calibration that makes a user request (α^*, δ) operationally precise for the *single deployed predictor* obtained after one calibration draw. SSBC selects a conformal grid index (equivalently an order statistic) so that, with probability at least $1 - \delta$ over calibration randomness, the realized coverage of the deployed rule is at least $1 - \alpha^*$. In the finite-window variant, the same guarantee is imposed on empirical coverage over a future window of size m . The construction relies only on the exact finite-sample law of calibration-conditional coverage from Appendix B.

C.1 Setup and conformal grid

Let n_{cal} be the calibration size and let $S_i := s(X_i, Y_i)$ denote true-label nonconformity scores for $i = 1, \dots, n_{\text{cal}}$. Split conformal selects a threshold as an order statistic:

$$\tau = S_{(k)}, \quad k \in \{1, \dots, n_{\text{cal}}\}.$$

It is convenient to re-index the same grid by the miscoverage index

$$u := n_{\text{cal}} + 1 - k \in \{1, \dots, n_{\text{cal}}\}, \quad \alpha_{\text{grid}} = \frac{u}{n_{\text{cal}} + 1}, \quad k = n_{\text{cal}} + 1 - u.$$

Here $\alpha^* \in (0, 1)$ is the requested miscoverage and $\delta \in (0, 1)$ is a confidence/risk level controlling the probability (over calibration draws) that the requested semantics fail.

C.2 Exact law of realized (calibration-conditional) coverage

For the fixed predictor calibrated on \mathcal{D}_{cal} , define the calibration-conditional coverage probability

$$p_{\text{cov}}(\mathcal{D}_{\text{cal}}) := \mathbb{P}(S_{n+1} \leq \tau \mid \mathcal{D}_{\text{cal}}),$$

where (X_{n+1}, Y_{n+1}) is exchangeable with the calibration sample. Under exchangeability, Appendix B shows that

$$p_{\text{cov}}(\mathcal{D}_{\text{cal}}) \sim \text{Beta}(k, u), \quad k = n_{\text{cal}} + 1 - u,$$

exactly and distribution-free. This law describes how the realized coverage of the deployed predictor varies across hypothetical recalibrations, while treating the deployed rule as fixed after the one calibration step.

C.3 SSBC objective: calibration-conditional PAC semantics

SSBC enforces the calibration-conditional PAC-style constraint

$$\mathbb{P}_{\mathcal{D}_{\text{cal}}}(p_{\text{cov}}(\mathcal{D}_{\text{cal}}) \geq 1 - \alpha^*) \geq 1 - \delta.$$

Using the Beta law, this is equivalent to

$$\mathbb{P}(Z \geq 1 - \alpha^*) \geq 1 - \delta, \quad Z \sim \text{Beta}(k, u).$$

Selection rule (least conservative admissible grid point). Among discrete grid indices $u \in \{1, \dots, n_{\text{cal}}\}$, SSBC selects the *largest admissible* u satisfying the tail constraint above:

$$u^* := \max \left\{ u \in \{1, \dots, n_{\text{cal}}\} : \mathbb{P}(Z \geq 1 - \alpha^*) \geq 1 - \delta, Z \sim \text{Beta}(n_{\text{cal}} + 1 - u, u) \right\}.$$

Equivalently, SSBC deploys the least conservative grid miscoverage level $\alpha_{\text{adj}} = u^*/(n_{\text{cal}} + 1)$ that certifies the requested semantics. The returned order-statistic index is $k_{\text{adj}} = n_{\text{cal}} + 1 - u^*$.

C.4 Finite-window deployment semantics

In many deployments, coverage is evaluated over a finite window of size m . Define empirical coverage over that window by

$$\widehat{C}_m := \frac{1}{m} \sum_{j=1}^m I_{\text{cov},j}, \quad I_{\text{cov},j} := \mathbf{1}\{Y'_j \in C(X'_j)\}, \quad S_m := m\widehat{C}_m.$$

Conditional on the calibration-conditional coverage probability $p_{\text{cov}}(\mathcal{D}_{\text{cal}}) = p$,

$$S_m \mid p \sim \text{Binomial}(m, p).$$

Marginalizing $p \sim \text{Beta}(k, u)$ yields the exact mixture law

$$S_m \sim \text{Beta-Binomial}(m; k, u), \quad k = n_{\text{cal}} + 1 - u.$$

The finite-window SSBC criterion selects u such that

$$\mathbb{P}(\widehat{C}_m \geq 1 - \alpha^*) \geq 1 - \delta,$$

where the probability is over both calibration randomness and the future window.

C.4.1 Strict lower-tail convention

Because \widehat{C}_m is discrete, we adopt a strict violation convention $\widehat{C}_m < 1 - \alpha^*$. Define the corresponding count threshold

$$x^* := \lfloor (1 - \alpha^*)m \rfloor + 1, \quad \text{so that} \quad \{\widehat{C}_m \geq 1 - \alpha^*\} \iff \{S_m \geq x^*\}.$$

All Beta–Binomial tail probabilities in SSBC are evaluated for the event $\{S_m \geq x^*\}$. This avoids boundary ambiguity when $(1 - \alpha^*)m$ is an integer and preserves monotonicity in u .

C.5 Infinite-window limit

Proposition 2 (Infinite-window limit of SSBC). *Fix n_{cal} , α^* , and δ . Let u_m be the SSBC-selected index obtained by inverting the Beta–Binomial tail for window size m , and let u_∞ be the SSBC-selected index obtained by inverting the Beta tail. Then*

$$u_m \longrightarrow u_\infty \quad \text{as } m \rightarrow \infty.$$

Proof sketch. Conditional on $p_{\text{cov}} = p$, $\widehat{C}_m \rightarrow p$ almost surely as $m \rightarrow \infty$. Therefore the Beta–Binomial mixture converges weakly to the Beta law for p_{cov} , and the corresponding admissibility conditions for grid points converge. \square

C.6 Feasibility and saturation

Not every pair (α^*, δ) is feasible at fixed n_{cal} because calibration choices lie on the conformal grid. Under the most conservative grid point $u = 1$ (equivalently $k = n_{\text{cal}}$),

$$p_{\text{cov}} \sim \text{Beta}(n_{\text{cal}}, 1), \quad \mathbb{P}(p_{\text{cov}} \geq 1 - \alpha) = 1 - (1 - \alpha)^{n_{\text{cal}}}.$$

Thus any infinite-window PAC requirement at confidence $1 - \delta$ must satisfy

$$\alpha \geq 1 - \delta^{1/n_{\text{cal}}}.$$

If this condition is violated (and likewise in the finite-window analogue), no grid point can satisfy the tail constraint and SSBC returns INFEASIBLE.

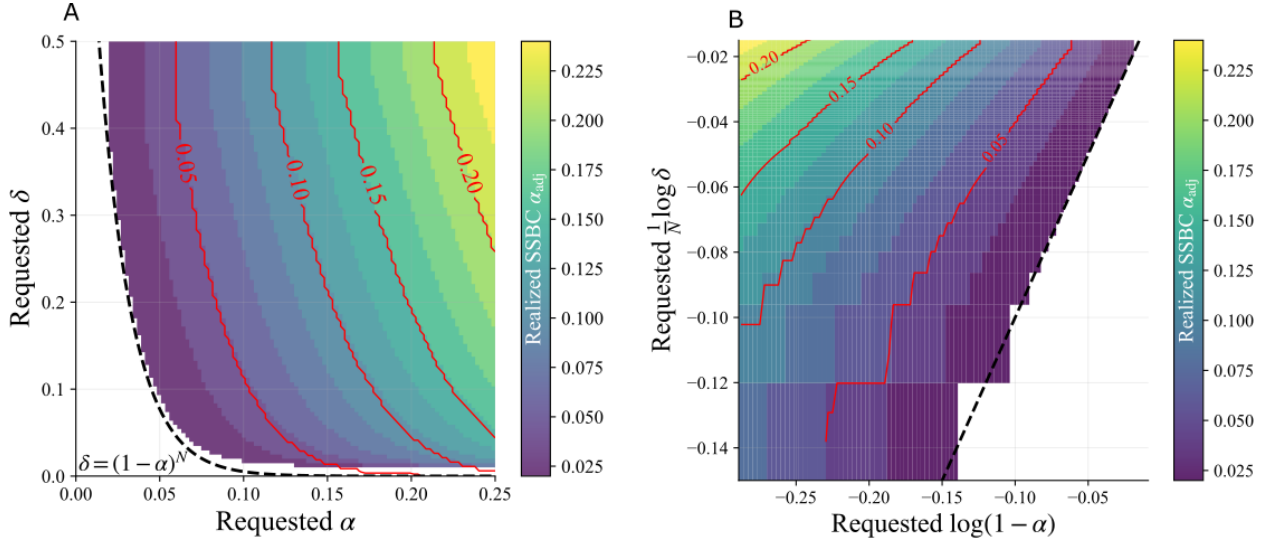


Figure 6: **Semantic interpretation of nominal coverage requests under finite calibration.** Each panel visualizes the effective calibration level α_{adj} selected by SSBC as a function of the user-specified miscoverage level α and confidence level δ , for fixed n_{cal} . Color encodes the deployed level α_{adj} , while contours indicate iso-semantic sets: distinct nominal requests that induce the same deployed calibration grid point. The feasibility boundary reflects the finite-sample constraint $\alpha \gtrsim 1 - \delta^{1/n_{\text{cal}}}$.

C.7 Coverage semantics under finite calibration

To visualize how nominal requests map to deployed semantics under finite calibration, Figure 6 plots the effective calibration level α_{adj} selected by SSBC as a function of the user inputs (α, δ) at fixed n_{cal} . Distinct nominal requests can induce the same deployed grid index and therefore the same realized coverage semantics.

C.8 SSBC algorithm (deterministic specification)

This subsection provides a reproducible implementation-level specification. The algorithm returns the largest admissible u (least conservative grid point) satisfying the relevant tail constraint.

Relation to DKWM-style calibration. DKWM-style calibration modifies the nominal grid choice to enforce conservative, worst-case guarantees uniformly over calibration draws and distributions. SSBC addresses a different question: it assigns a calibration-conditional PAC meaning to a user request (α^*, δ) for the *single deployed* predictor produced after one calibration. DKWM targets uniform validity across hypothetical recalibrations; SSBC targets admissibility of the realized rule via exact Beta (or Beta-Binomial) tails.

C.9 Extended simulation table for calibration-conditional violations

Table 7 reports the full calibration-size grid for the simulation summarized in Section 5.1.1.

D Single-sample structural coupling, leave-one-out decoupling, and envelope inflation

The two-stage predictive reference used throughout this paper separates *calibration* (choose a conformal threshold on \mathcal{D}_{cal}) from *operational evaluation* (estimate rates on an independent window). This separation is what makes window indicators behave as i.i.d. Bernoulli draws under a fixed deployed rule.

Table 7: **Calibration-conditional coverage violation rates with theory.** Target miscoverage $\alpha^* = 0.10$, confidence $\delta = 0.10$. α_{grid} is the grid point selected on the conformal grid, α_{cont} is the requested value under the DKWM correction, and m_{cal} is the calibration-window size. Results are based on 10^6 calibration draws and a finite deployment window of size $m_{\text{infer}} = 100$. The **Obs** column reports $\mathbb{P}(\widehat{C}_m < 1 - \alpha^*)$. **BetaTheory** reports $\mathbb{P}(p_{\text{cov}} < 1 - \alpha^*)$ under $p_{\text{cov}} \sim \text{Beta}(k, u)$. **BBTheory** reports $\mathbb{P}(\widehat{C}_m < 1 - \alpha^*)$ under the induced Beta–Binomial law.

n_{cal}	Method	u	α_{grid}	Obs	BetaTheory	BBTheory	α_{cont}
50	None	5	0.0980	0.3963	0.4312	0.3964	–
50	SSBC	2	0.0392	0.0476	0.0338	0.0472	–
50	DKWM	1	0.0196	0.0096	0.0052	0.0095	–0.0731
75	None	7	0.0921	0.3454	0.3673	0.3464	–
75	SSBC	4	0.0526	0.0769	0.0504	0.0768	–
75	DKWM	1	0.0132	0.0016	0.0004	0.0017	–0.0413
100	None	10	0.0990	0.4075	0.4513	0.4071	–
100	SSBC	6	0.0594	0.0960	0.0576	0.0956	–
100	DKWM	1	0.0099	0.0004	0.0000	0.0004	–0.0224
150	None	15	0.0993	0.4119	0.4602	0.4107	–
150	SSBC	9	0.0596	0.0804	0.0307	0.0801	–
150	DKWM	1	0.0066	0.0000	0.0000	0.0000	+0.0001
200	None	20	0.0995	0.4130	0.4655	0.4124	–
200	SSBC	13	0.0647	0.0974	0.0320	0.0980	–
200	DKWM	2	0.0100	0.0000	0.0000	0.0000	+0.0135
250	None	25	0.0996	0.4126	0.4692	0.4134	–
250	SSBC	16	0.0637	0.0863	0.0175	0.0858	–
250	DKWM	5	0.0199	0.0003	0.0000	0.0003	+0.0226
300	None	30	0.0997	0.4139	0.4719	0.4141	–
300	SSBC	20	0.0664	0.0969	0.0171	0.0971	–
300	DKWM	8	0.0266	0.0009	0.0000	0.0009	+0.0293
500	None	50	0.0998	0.4153	0.4782	0.4153	–
500	SSBC	34	0.0679	0.0949	0.0049	0.0955	–
500	DKWM	22	0.0439	0.0097	0.0000	0.0096	+0.0453

Algorithm 1 Small-Sample Beta Correction (SSBC)

Require: Target miscoverage $\alpha^* \in (0, 1)$; calibration size $n_{\text{cal}} \in \mathbb{N}$; confidence $\delta \in (0, 1)$; deployment regime $\in \{\infty, m\}$ (window size m if finite)

Ensure: Adjusted grid level α_{adj} and index k_{adj} , or INFEASIBLE

```
1:  $t \leftarrow 1 - \alpha^*$ 
2:  $u^* \leftarrow -1$ 
3: if regime =  $m$  then
4:    $x^* \leftarrow \lfloor tm \rfloor + 1$ 
5: end if
6: for  $u = 1, \dots, n_{\text{cal}}$  do
7:    $a \leftarrow n_{\text{cal}} + 1 - u, \quad b \leftarrow u$ 
8:   if regime =  $\infty$  then
9:      $p_{\text{tail}} \leftarrow \Pr[Z \geq t], \quad Z \sim \text{Beta}(a, b)$ 
10:  else
11:     $p_{\text{tail}} \leftarrow \Pr[X \geq x^*], \quad X \sim \text{Beta-Binomial}(m; a, b)$ 
12:  end if
13:  if  $p_{\text{tail}} \geq 1 - \delta$  then
14:     $u^* \leftarrow u$ 
15:  end if
16: end for
17: if  $u^* < 0$  then
18:   return INFEASIBLE
19: end if
20:  $\alpha_{\text{adj}} \leftarrow \frac{u^*}{n_{\text{cal}} + 1}$ 
21:  $k_{\text{adj}} \leftarrow n_{\text{cal}} + 1 - u^*$ 
22: return  $\alpha_{\text{adj}}, k_{\text{adj}}$ 
```

In practice, an independent audit window is often unavailable. When the same sample is reused both to select the threshold and to estimate operational rates, threshold selection and evaluation become coupled. This appendix records (i) a minimal structural reason for reuse-induced dependence, (ii) a data-efficient remedy—leave-one-out (LOO) recalibration—that provides effective *practical decoupling* in our regimes, and (iii) an *inflation* parameter `infl` that pessimizes predictive envelopes when residual dependence or regime instability remains.

D.1 Why single-sample reuse introduces dependence

Let $\mathcal{D}_{\text{cal}} = \{(X_i, Y_i)\}_{i=1}^n$ be an exchangeable calibration sample, let $S_i := s(X_i, Y_i)$ be true-label nonconformity scores, and let the split conformal threshold be the k th order statistic

$$\hat{\tau} := S_{(k)}, \quad k \in \{1, \dots, n\},$$

assuming continuity so ties occur with probability zero. For any threshold t , define the crossing indicator $I_i(t) := \mathbf{1}\{S_i \leq t\}$.

Lemma 3 (Order-statistic coupling under reuse). *Assume S_1, \dots, S_n are exchangeable and continuous, and let $\hat{\tau} = S_{(k)}$. Then, conditional on $\hat{\tau} = t$,*

$$\sum_{i=1}^n I_i(t) = k \quad \text{almost surely.}$$

Consequently, $\{I_i(t)\}_{i=1}^n$ are not conditionally independent given $\hat{\tau} = t$, and for any $i \neq j$,

$$\text{Cov}(I_i(t), I_j(t) \mid \hat{\tau} = t) = \frac{k(k-n)}{n^2(n-1)} < 0 \quad (k < n).$$

Proof. Conditioning on $\hat{\tau} = t$ fixes exactly $k - 1$ scores strictly below t and one score equal to t , hence $\sum_{i=1}^n I_i(t) = k$ deterministically. The covariance identity follows from exchangeability and counting. \square

Implication for operational envelopes. Operational indicators are functions of the deployed prediction set $C_{\hat{\tau}}(X) = \{y : s(X, y) \leq \hat{\tau}\}$ and therefore inherit reuse-induced dependence. If one naïvely treats reuse-based indicators as i.i.d. Bernoulli under a fixed rule, predictive envelopes can become under-dispersed. Empirically in our studies, the dominant distortion is in *dispersion*: point estimates often remain close to a two-stage reference, while intervals can be too narrow without decoupling or pessimization.

D.2 Approximate decoupling via leave-one-out (LOO)

When an independent audit sample is unavailable, we use LOO recalibration (Vovk, 2015; Barber et al., 2021) to reduce self-influence. Let $\hat{\tau}_{-i}$ be the split conformal threshold computed on $\mathcal{D}_{\text{cal}} \setminus \{(X_i, Y_i)\}$, and let $C_{-i}(\cdot)$ be the corresponding prediction set map. For an operational event functional $g_j(C(X), Y) \in \{0, 1\}$ (e.g., singleton, doublet, wrong-singleton), define LOO indicators

$$Z_{i,j} := g_j(C_{-i}(X_i), Y_i), \quad i = 1, \dots, n,$$

and pooled LOO summaries

$$k_{\text{pool},j} := \sum_{i=1}^n Z_{i,j}, \quad \hat{r}_j^{\text{LOO}} := \frac{k_{\text{pool},j}}{n}.$$

Proxy two-stage interpretation. Each $Z_{i,j}$ is evaluated under a rule that does not use point i , restoring a localized separation between rule construction and evaluation. Although the rule varies across folds, each fold differs only slightly from the full calibrated rule, so $\{Z_{i,j}\}$ can be read as indicators from nearby operating regimes. Pooling provides a direct empirical proxy for operational behavior under finite calibration.

Empirical decoupling. In the regimes studied (Section 5.1.2), LOO envelopes track the two-stage Calibrate-and-Audit reference closely in center and often slightly pessimistically in width. We therefore use pooled LOO indicators for planning when a separate audit set is unavailable.

D.3 Envelope inflation as controlled pessimization

LOO is local and does not remove all dependence, especially near regime boundaries where small threshold shifts can change region support. We therefore introduce an explicit inflation parameter $\text{infl} \geq 1$ that widens predictive envelopes by shrinking an effective sample size used in the predictive model.

Operational effect. In constructions below we replace a nominal proxy sample size n by $n_{\text{eff}} = n/\text{infl}$ (and analogously for any proxy count used to parameterize predictive dispersion). Larger infl yields wider envelopes without changing the pooled mean, providing a monotone knob for conservatism.

Diagnostic guidance (optional). As a simple diagnostic of calibration-induced variability, one can compute fold rates $\hat{r}^{(-i)}$ under each LOO-calibrated rule and their empirical variance

$$\bar{r}_{\text{LOO}} = \frac{1}{n} \sum_{i=1}^n \hat{r}^{(-i)}, \quad \widehat{\text{Var}}_{\text{LOO}} = \frac{1}{n-1} \sum_{i=1}^n \left(\hat{r}^{(-i)} - \bar{r}_{\text{LOO}} \right)^2.$$

In our experiments this variance aligns qualitatively with inflation levels needed for conservative envelope coverage relative to the two-stage reference.

D.4 Predictive envelope constructions from LOO proxies

We describe two complementary envelope constructions built from LOO proxy indicators. The first mirrors the two-stage reference and is our primary approximation; the second is a conservative guardrail.

Predictive Beta–Binomial envelopes (primary approximation). Let Z_i denote a pooled proxy indicator for a fixed KPI (suppress j), and let $k_{\text{pool}} = \sum_{i=1}^n Z_i$ with pooled proxy rate $\hat{p} = k_{\text{pool}}/n$. Apply inflation via

$$n_{\text{eff}} = \frac{n}{\text{infl}}, \quad k_{\text{eff}} = \hat{p}n_{\text{eff}} = \frac{k_{\text{pool}}}{\text{infl}}.$$

With a small prior offset $\text{offset} \in \{1, 1/2\}$, define

$$\alpha := k_{\text{eff}} + \text{offset}, \quad \beta := (n_{\text{eff}} - k_{\text{eff}}) + \text{offset}.$$

For a future deployment window of size m , the predictive count S_m is modeled as

$$S_m \sim \text{BetaBinomial}(m, \alpha, \beta),$$

and equal-tailed prediction intervals follow from the Beta–Binomial CDF. Increasing `infl` shrinks n_{eff} and widens intervals monotonically while preserving the pooled mean.

Hoeffding-type dominance bound (guardrail). As a conservative alternative, Hoeffding’s inequality gives a distribution-free bound for a window rate \hat{r}_m around a proxy mean \hat{r}_{LOO} :

$$\Pr(|\hat{r}_m - \hat{r}_{\text{LOO}}| \geq \epsilon) \leq 2 \exp(-2m\epsilon^2),$$

yielding simple symmetric envelopes that can be used as a worst-case planning check.

Summary. Single-sample reuse induces structural dependence through order-statistic thresholding (Lemma 3), primarily distorting predictive *dispersion*. LOO recalibration reduces self-influence and empirically recovers audit-style behavior in our regimes. Predictive envelopes are then constructed from pooled LOO proxies using a Beta–Binomial model, with `infl` providing a monotone knob for controlled pessimization and a Hoeffding bound serving as a conservative guardrail.

E Binary conformal partitions: regimes, coupling, and rate primitives

This appendix records the geometric facts used in Section 2, Section 3, and Section 4. We work in the *calibration-conditional* viewpoint: thresholds are treated as fixed (conditional on the realized calibration draw), and all probabilities are taken with respect to the deployment distribution conditional on \mathcal{D}_{cal} .

E.1 Mondrian split conformal as a four-region partition

Let $\mathcal{Y} = \{0, 1\}$ and let $s(x, y)$ be a nonconformity score. Mondrian (class-conditional) split conformal produces thresholds τ_0, τ_1 , and the set-valued output is

$$\mathcal{C}(x) = \{0 : s(x, 0) \leq \tau_0\} \cup \{1 : s(x, 1) \leq \tau_1\}, \quad (2)$$

equivalently represented by the region label

$$R_\tau(x) := (\mathbf{1}\{s(x, 0) \leq \tau_0\}, \mathbf{1}\{s(x, 1) \leq \tau_1\}) \in \{0, 1\}^2, \quad \tau = (\tau_0, \tau_1).$$

Writing $(s_0, s_1) = (s(x, 0), s(x, 1))$, the thresholds partition score space into

$$R_\tau(x) = \begin{cases} 11, & s_0 \leq \tau_0, s_1 \leq \tau_1 & \text{(doublet)}, \\ 10, & s_0 \leq \tau_0, s_1 > \tau_1 & \text{(singleton } \{0\}\text{)}, \\ 01, & s_0 > \tau_0, s_1 \leq \tau_1 & \text{(singleton } \{1\}\text{)}, \\ 00, & s_0 > \tau_0, s_1 > \tau_1 & \text{(abstention)}. \end{cases}$$

For any fixed τ ,

$$\sum_{r \in \{00, 01, 10, 11\}} \mu_r(\tau) = 1, \quad \mu_r(\tau) := \Pr(R_\tau(X) = r \mid \mathcal{D}_{\text{cal}}).$$

E.2 Probability-normalized scores and a sharp regime boundary

Many probabilistic classifiers induce probability-normalized scores, e.g. $s(x, y) = 1 - P(y | x)$. For $\mathcal{Y} = \{0, 1\}$ this implies

$$s(x, 0) + s(x, 1) = 1,$$

so feasible score pairs lie on the diagonal manifold

$$\mathcal{M} = \{(u, 1 - u) : u \in [0, 1]\}.$$

Intersecting \mathcal{M} with the threshold rectangles yields a sharp boundary that determines which region types can occur with nonzero mass.

Proposition 4 (Regime boundary under probability normalization). *Assume $(s_0, s_1) \in \mathcal{M}$ almost surely. Then:*

1. R_{11} has nonempty intersection with \mathcal{M} iff $\tau_0 + \tau_1 \geq 1$, and has positive-length intersection iff $\tau_0 + \tau_1 > 1$.
2. R_{00} has nonempty intersection with \mathcal{M} iff $\tau_0 + \tau_1 \leq 1$, and has positive-length intersection iff $\tau_0 + \tau_1 < 1$.
3. On the boundary $\tau_0 + \tau_1 = 1$, both R_{11} and R_{00} intersect \mathcal{M} at a single point; hence under any continuous distribution on \mathcal{M} they have probability zero and only the singleton regions carry mass.

Proof. Parameterize \mathcal{M} by $u = s_0 \in [0, 1]$, so $s_1 = 1 - u$.

R_{11} requires $u \leq \tau_0$ and $1 - u \leq \tau_1$, i.e. $u \in [1 - \tau_1, \tau_0]$. This interval has positive length iff $1 - \tau_1 < \tau_0$, i.e. $\tau_0 + \tau_1 > 1$, and degenerates to a point at equality.

R_{00} requires $u > \tau_0$ and $1 - u > \tau_1$, i.e. $u \in (\tau_0, 1 - \tau_1)$. This interval has positive length iff $\tau_0 < 1 - \tau_1$, i.e. $\tau_0 + \tau_1 < 1$, and degenerates to a point at equality. \square

Crossing the affine boundary $\tau_0 + \tau_1 = 1$ therefore removes an entire region label (doublet or abstention) from the support of $R_\tau(X)$ under probability normalization, explaining sharp regime changes in attainable operating behavior.

E.3 Cross-threshold dominance in the hedging regime

Within the hedging regime $\tau_0 + \tau_1 > 1$, the manifold \mathcal{M} is partitioned into three contiguous intervals corresponding to $\{10, 11, 01\}$. With $u = s(x, 0)$:

$$u \in [0, 1 - \tau_1) \Rightarrow R_\tau(x) = 10, \quad u \in [1 - \tau_1, \tau_0] \Rightarrow R_\tau(x) = 11, \quad u \in (\tau_0, 1] \Rightarrow R_\tau(x) = 01.$$

Hence each singleton region is controlled primarily by the *opposing* threshold: increasing τ_1 expands 11 at the expense of 10, while increasing τ_0 expands 11 at the expense of 01. Operationally, (τ_0, τ_1) act as *mass-reallocation boundaries*, not independent per-class knobs.

E.4 Region-label primitives and rate factorizations

For auditing and planning, the primitive object is the region-label table

$$p_{r,y}(\tau) := \Pr(R_\tau(X) = r, Y = y | \mathcal{D}_{\text{cal}}), \quad r \in \{00, 01, 10, 11\}, \quad y \in \{0, 1\}.$$

Two derived summaries are

$$\mu_r(\tau) := \Pr(R_\tau(X) = r | \mathcal{D}_{\text{cal}}) = \sum_{y \in \{0, 1\}} p_{r,y}(\tau), \quad \eta_r(\tau) := \Pr(Y = 1 | R_\tau(X) = r, \mathcal{D}_{\text{cal}}) = \frac{p_{r,1}(\tau)}{\mu_r(\tau)} \quad (\mu_r(\tau) > 0).$$

Any region-measurable KPI is a projection of $\{p_{r,y}(\tau)\}$; see Section 2.4.

Example: decisive error masses under “commit-on-singletons”. Consider the convention

$$10 \mapsto 0, \quad 01 \mapsto 1, \quad 11, 00 \mapsto \text{defer}.$$

Then the decisive false-negative and false-positive masses are

$$\text{FN}_{\text{dec}}(\tau) = \Pr(R_\tau(X) = 10, Y = 1 \mid \mathcal{D}_{\text{cal}}) = p_{10,1}(\tau) = \mu_{10}(\tau) \eta_{10}(\tau),$$

$$\text{FP}_{\text{dec}}(\tau) = \Pr(R_\tau(X) = 01, Y = 0 \mid \mathcal{D}_{\text{cal}}) = p_{01,0}(\tau) = \mu_{01}(\tau) [1 - \eta_{01}(\tau)].$$

The decisive mass is $\mu_{10}(\tau) + \mu_{01}(\tau)$, while the defer mass is $\mu_{11}(\tau) + \mu_{00}(\tau)$ (with feasibility of 11 versus 00 governed by Proposition 4 under probability normalization).

F Cost-coherence and inverse pricing envelopes induced by a fixed conformal interface

This appendix formalizes the operational point that distribution-free calibration is not automatically cost-agnostic once conformal outputs are wired into actions. Fix thresholds τ (calibration-conditional viewpoint) and treat the induced finite region label $R_\tau(X) \in \mathcal{R}$ as the deployed observable. Any downstream rule that uses only this interface can depend on the data only through $r \in \mathcal{R}$, so whether the convention is coherent with a cost model is evaluated *region-wise* using within-region label frequencies (we formalize this as *cost-coherence* below). We cast this as an *inverse pricing* problem: given a fixed (interface, convention) pair, characterize the set of consequence prices under which the convention is coherent.

F.1 Interface primitives: masses and within-region label frequencies

Specialize to $\mathcal{Y} = \{0, 1\}$ and $\mathcal{R} = \{00, 01, 10, 11\}$ as in Appendix E. Adopt the calibration-conditional joint table

$$p_{r,y} := \Pr(R_\tau(X) = r, Y = y \mid \mathcal{D}_{\text{cal}}).$$

Define region mass and within-region label frequency

$$\mu_r := p_{r,0} + p_{r,1}, \quad \eta_r := \Pr(Y = 1 \mid R_\tau(X) = r, \mathcal{D}_{\text{cal}}) = \frac{p_{r,1}}{\mu_r} \quad (\mu_r > 0).$$

Because \mathcal{R} is finite, conditional uncertainty about Y is piecewise constant: within region r , all decision comparisons reduce to η_r .

F.2 Region-measurable action conventions and coherence

Let \mathcal{A} be a finite action set and let $L_\theta(a, y)$ be a priced consequence (cost or negative utility), parameterized by $\theta \in \Theta$. A deployed convention is a region-measurable policy

$$\tilde{\pi} : \mathcal{R} \rightarrow \mathcal{A}.$$

For region r with $\mu_r > 0$, the interface-relative conditional risk of action a is

$$\mathcal{C}_\theta(a \mid r) := \mathbb{E}[L_\theta(a, Y) \mid R_\tau(X) = r, \mathcal{D}_{\text{cal}}] = (1 - \eta_r)L_\theta(a, 0) + \eta_r L_\theta(a, 1).$$

Cost-coherence (interface-relative optimality). We say $\tilde{\pi}$ is *cost-coherent* on the deployed interface under pricing θ if for every region with $\mu_r > 0$,

$$\mathcal{C}_\theta(\tilde{\pi}(r) \mid r) \leq \mathcal{C}_\theta(a \mid r) \quad \forall a \in \mathcal{A}.$$

This is the dominance condition induced by acting only on $R_\tau(X)$.

F.3 Inverse pricing envelope

For each region with $\mu_r > 0$, define the local feasibility set

$$\Theta_r(\tilde{\pi}) := \left\{ \theta \in \Theta : \mathcal{C}_\theta(\tilde{\pi}(r) \mid r) \leq \mathcal{C}_\theta(a \mid r) \quad \forall a \in \mathcal{A} \right\},$$

and the global pricing envelope

$$\Theta(\tilde{\pi}) := \bigcap_{r: \mu_r > 0} \Theta_r(\tilde{\pi}).$$

Equivalently, $\Theta(\tilde{\pi})$ is the set of price parameters for which the forced action in each region is cost-coherent given only the conformal output. Since only action comparisons matter, envelopes are naturally reported in ratio (projective) coordinates: global positive scaling of L_θ is irrelevant, and adding offsets b_y independent of a preserves comparisons.

F.4 Worked case: Chow-style reject option and “commit on singletons”

Consider $\mathcal{A} = \{0, 1, \text{rej}\}$ with Chow-style costs (false negative $c_{01} > 0$, false positive $c_{10} > 0$, rejection $c_{\text{rej}} \geq 0$):

$$L(0, 1) = c_{01}, \quad L(1, 0) = c_{10}, \quad L(\text{rej}, y) = c_{\text{rej}}, \quad L(0, 0) = L(1, 1) = 0.$$

In region r the conditional risks are

$$\mathcal{C}(0 \mid r) = \eta_r c_{01}, \quad \mathcal{C}(1 \mid r) = (1 - \eta_r) c_{10}, \quad \mathcal{C}(\text{rej} \mid r) = c_{\text{rej}}.$$

Work in ratios

$$\lambda := \frac{c_{01}}{c_{10}}, \quad \rho := \frac{c_{\text{rej}}}{c_{10}},$$

so only (λ, ρ) matters for comparisons.

Convention.

$$\tilde{\pi}(10) = 0, \quad \tilde{\pi}(01) = 1, \quad \tilde{\pi}(11) = \text{rej}, \quad \tilde{\pi}(00) = \text{rej}.$$

Coherence holds iff the region-wise dominance inequalities below hold for all regions with $\mu_r > 0$.

Singleton region 01 (output {1}). Choosing 1 must beat both 0 and rej:

$$(1 - \eta_{01}) \leq \eta_{01} \lambda \iff \eta_{01} \geq \frac{1}{1 + \lambda}, \quad (1 - \eta_{01}) \leq \rho \iff \eta_{01} \geq 1 - \rho.$$

Thus

$$\eta_{01} \geq \max \left\{ \frac{1}{1 + \lambda}, 1 - \rho \right\}.$$

Singleton region 10 (output {0}). Choosing 0 must beat both 1 and rej:

$$\eta_{10} \lambda \leq (1 - \eta_{10}) \iff \eta_{10} \leq \frac{1}{1 + \lambda}, \quad \eta_{10} \lambda \leq \rho \iff \eta_{10} \leq \frac{\rho}{\lambda}.$$

Thus

$$\eta_{10} \leq \min \left\{ \frac{1}{1 + \lambda}, \frac{\rho}{\lambda} \right\}.$$

Rejection regions $r \in \{11, 00\}$. Rejecting must beat both commitments:

$$\rho \leq \eta_r \lambda \iff \eta_r \geq \frac{\rho}{\lambda}, \quad \rho \leq (1 - \eta_r) \iff \eta_r \leq 1 - \rho.$$

Hence rejection is optimal on region r only if

$$\frac{\rho}{\lambda} \leq \eta_r \leq 1 - \rho.$$

The rejection band is nonempty only if

$$\frac{\rho}{\lambda} \leq 1 - \rho \iff \rho \leq \frac{\lambda}{1 + \lambda} \iff c_{\text{rej}} \leq \frac{c_{01}c_{10}}{c_{01} + c_{10}}.$$

The inequalities above depend only on the interface primitives $\{\eta_r\}$ (and on which regions have $\mu_r > 0$). Thus, for a fixed calibrated conformal predictor and a fixed wiring convention $\tilde{\pi}$, coherence restricts the admissible cost ratios (λ, ρ) . Equivalently, (λ, ρ) defines half-space constraints in the plane whose intersection is the pricing envelope $\Theta(\tilde{\pi})$ (possibly empty). This is the operational content of (C3): calibration is distribution-free, but coherent downstream use is constrained by the coarse information carried by the conformal partition.

G Explicit region indicators and projection masks

This appendix instantiates the linear “sum selected cells” formalism from Section 2.4 in the binary toy geometry used in Figure 2 and Figure 3 ($R_\tau(x) \xrightarrow{\pi} C(x)$). Region feasibility and regime facts are recorded in Appendix E; here we keep only the explicit projection masks used in audit computations.

G.1 Region labels and the region–label table

Assume $\mathcal{Y} = \{0, 1\}$ and thresholds $\tau = (\tau_0, \tau_1)$. Define the deployed region label

$$R_\tau(x) = (r_0(x), r_1(x)) \in \{0, 1\}^2, \quad r_y(x) := \mathbf{1}\{s(x, y) \leq \tau_y\},$$

with region names $\mathcal{R} = \{r_{10}, r_{11}, r_{01}, r_{00}\}$ as in Appendix E.1. For a calibration setting θ (indexing deployed thresholds $\tau(\theta)$), define the calibration-conditional region–label table

$$P(\theta) = (p_{r,y}(\theta))_{r \in \mathcal{R}, y \in \mathcal{Y}}, \quad p_{r,y}(\theta) = \Pr(R_{\tau(\theta)}(X) = r, Y = y \mid \mathcal{D}_{\text{cal}}).$$

A linear operational rate is obtained by summing the subset of cells (r, y) that define the event.

G.2 Policies used in Figure 3

A policy π maps region labels to prediction sets $C(x) \subseteq \{0, 1\}$:

$$R_\tau(x) \xrightarrow{\pi} C(x).$$

The three policies used in Figure 3 are:

Set inclusion π_{SI} .

$$\pi_{\text{SI}}(r_{10}) = \{0\}, \quad \pi_{\text{SI}}(r_{11}) = \{0, 1\}, \quad \pi_{\text{SI}}(r_{01}) = \{1\}, \quad \pi_{\text{SI}}(r_{00}) = \emptyset.$$

Commit–reject π_{CR} .

$$\pi_{\text{CR}}(r_{10}) = \{0\}, \quad \pi_{\text{CR}}(r_{01}) = \{1\}, \quad \pi_{\text{CR}}(r_{11}) = \emptyset, \quad \pi_{\text{CR}}(r_{00}) = \emptyset.$$

Set exclusion π_{SE} (complement of set inclusion).

$$\pi_{\text{SE}}(r_{10}) = \{1\}, \quad \pi_{\text{SE}}(r_{11}) = \emptyset, \quad \pi_{\text{SE}}(r_{01}) = \{0\}, \quad \pi_{\text{SE}}(r_{00}) = \{0, 1\}.$$

G.3 Binary projection masks

Fix a policy π . For any event/quantity ℓ , define a 4×2 binary mask

$$G_{\ell}(\pi) = (g_{\ell}(r, y; \pi))_{r \in \mathcal{R}, y \in \mathcal{Y}} \in \{0, 1\}^{4 \times 2},$$

where $g_{\ell}(r, y; \pi) = 1$ indicates that the cell (r, y) is included in the sum. Then the corresponding rate is

$$r_{\ell}(\theta) = \sum_{r \in \mathcal{R}} \sum_{y \in \mathcal{Y}} g_{\ell}(r, y; \pi) p_{r,y}(\theta).$$

We list four masks used repeatedly in the paper.

(1) Coverage under set inclusion. Under π_{SI} , coverage is the event $\{Y \in C(X)\}$. Cell-by-cell, coverage holds for: (i) $y = 0$ in regions r_{10} or r_{11} , and (ii) $y = 1$ in regions r_{01} or r_{11} . Hence

$$G_{\text{cov}}(\pi_{\text{SI}}) = \begin{array}{c|cc} & y = 0 & y = 1 \\ \hline r_{10} & 1 & 0 \\ r_{11} & 1 & 1 \\ r_{01} & 0 & 1 \\ r_{00} & 0 & 0 \end{array},$$

and therefore

$$r_{\text{cov}}(\theta) = p_{10,0}(\theta) + p_{11,0}(\theta) + p_{11,1}(\theta) + p_{01,1}(\theta).$$

Equivalently, coverage fails on the two singleton mistakes $(r_{10}, 1)$ and $(r_{01}, 0)$ and on all abstentions r_{00} .

(2) Missed positive mass (Figure 1: q_{10} under π_{SI}). In Figure 1, q_{10} is the positive-class mass in region r_{10} (output $\{0\}$ under π_{SI}):

$$q_{10}(\theta) = \Pr(Y = 1, C(X) = \{0\}) = \Pr(Y = 1, R_{\tau}(X) = r_{10}) = p_{10,1}(\theta),$$

with single-cell mask

$$G_{10}(\pi_{\text{SI}}) = \begin{array}{c|cc} & y = 0 & y = 1 \\ \hline r_{10} & 0 & 1 \\ r_{11} & 0 & 0 \\ r_{01} & 0 & 0 \\ r_{00} & 0 & 0 \end{array}.$$

(3) Hedged positive mass (Figure 1: q_{11} under π_{SI}). Similarly,

$$q_{11}(\theta) = \Pr(Y = 1, C(X) = \{0, 1\}) = \Pr(Y = 1, R_{\tau}(X) = r_{11}) = p_{11,1}(\theta),$$

with mask

$$G_{11}(\pi_{\text{SI}}) = \begin{array}{c|cc} & y = 0 & y = 1 \\ \hline r_{10} & 0 & 0 \\ r_{11} & 0 & 1 \\ r_{01} & 0 & 0 \\ r_{00} & 0 & 0 \end{array}.$$

(4) Abstention mass under the commit–reject policy. Under π_{CR} , abstention occurs in regions r_{11} and r_{00} , regardless of label. Thus

$$G_{\text{abs}}(\pi_{\text{CR}}) = \begin{array}{c|cc} & y = 0 & y = 1 \\ \hline r_{10} & 0 & 0 \\ r_{11} & 1 & 1 \\ r_{01} & 0 & 0 \\ r_{00} & 1 & 1 \end{array}$$

and

$$r_{\text{abs}}(\theta; \pi_{\text{CR}}) = (p_{11,0}(\theta) + p_{11,1}(\theta)) + (p_{00,0}(\theta) + p_{00,1}(\theta)).$$

G.4 Ratios of projections (conditional diagnostics)

Some diagnostics are conditional probabilities and therefore ratios of linear sums. For example, the purity of singleton-1 outputs under π_{SI} is

$$\text{Purity}_1(\theta) := \Pr(Y = 1 \mid C(X) = \{1\}) = \frac{\Pr(Y = 1, C(X) = \{1\})}{\Pr(C(X) = \{1\})} = \frac{p_{01,1}(\theta)}{p_{01,0}(\theta) + p_{01,1}(\theta)}.$$

Audit computation. All entries of $P(\theta)$ are estimated from region–label counts on the audit set. Linear KPIs are computed by summing selected cells; conditional diagnostics are computed as ratios of such sums.

H Tox21 supplementary details

This appendix provides supplementary documentation for the Tox21 experiments reported in Section 5.2. The purpose of this appendix is reproducibility and contextualization rather than extension of results or additional claims.

H.1 Tox21 dataset

The Tox21 benchmark consists of binary toxicity outcomes for twelve biological assays spanning nuclear receptor (NR) signaling and cellular stress response (SR) pathways. Each compound is labeled as *active* or *inactive* per assay. Labels are sparse and highly imbalanced, particularly for nuclear receptor targets.

The full dataset composition used in this study is reported in the main text (Table 2). We do not duplicate that table here.

H.2 Aggregated coverage summary

The aggregated coverage and prediction-set summary is reported in the main text (Table 3); we do not duplicate that table here.

H.3 Representative endpoint-level operational summaries

The SR-MMP endpoint summary is reported in the main text (Table 4). We keep one additional representative endpoint (NR-AR) here to document a complementary low-prevalence regime.

Because conformal calibration is performed in a class-conditional (Mondrian) manner, the effective calibration size for the positive class governs feasibility and discretization effects. Several assays operate with fewer than 100 positive calibration samples, placing them in the small-sample regime targeted by SSBC.

H.4 Representation and model protocol

All Tox21 experiments use a fixed, task-agnostic molecular representation (descriptors plus Morgan fingerprints) and a fixed CatBoost training protocol (1000 iterations, depth 6, learning rate 0.1, log-loss), with no

Table 8: **NR-AR endpoint.** Operational performance summary for the NR-AR endpoint. All reported quantities are joint probabilities normalized by the total test-set size. Rows report the singleton rate, doublet rate, and wrong-singleton rate ($P(Y = c, |S| = 1, \hat{y} \neq Y)$) by true class. "point estimate \mathcal{D}_1 " and "LOO 95% PI \mathcal{D}_1 " denote leave-one-out point estimates and their exact beta-binomial predictive intervals computed on the calibration data. "Observed \mathcal{D}_2 " reports empirical rates on an independent hold-out set. "BB 95% PI \mathcal{D}_2 " gives beta-binomial predictive intervals for the corresponding \mathcal{D}_2 quantities, accounting for calibration uncertainty and finite test size.

Operational quantity	Class	point estimate \mathcal{D}_1	LOO 95% PI \mathcal{D}_1	Observed \mathcal{D}_2	BB 95% PI \mathcal{D}_2
Singleton rate	Class 0	0.163	[0.125, 0.205]	0.133	[0.112, 0.157]
	Class 1	0.026	[0.011, 0.047]	0.029	[0.019, 0.041]
Doublet rate	Class 0	0.796	[0.751, 0.838]	0.818	[0.792, 0.843]
	Class 1	0.015	[0.005, 0.031]	0.020	[0.012, 0.030]
Wrong-singleton rate	Class 0	0.086	[0.058, 0.119]	0.060	[0.045, 0.077]
	Class 1	0.002	[0.000, 0.010]	0.001	[0.000, 0.004]

assay-specific feature engineering, class reweighting, or resampling. Molecules are parsed and sanitized using standard cheminformatics tooling, and compounds with invalid features are excluded. This intentionally non-optimized setup isolates conformal calibration and operational-envelope behavior from model-architecture tuning; observed AUROC values (approximately 0.80–0.85) are consistent with baseline Tox21 reports.

H.5 Conformal calibration and evaluation

All conformal predictors are calibrated in a class-conditional (Mondrian) fashion, with separate calibration sets for the positive and negative classes. For each run, one of three calibration strategies is applied: standard split conformal, DKWM-based correction, or SSBC, targeting $(\alpha, \delta) = (0.10, 0.10)$.

Calibration thresholds are computed once per run and evaluated on a held-out test set. Operational rates (singleton and doublet frequencies) are estimated using leave-one-out cross-validation on the calibration set. These LOO estimates are used to construct prediction intervals for future deployment batches of fixed size, as described in the main text.

I Solubility supplementary details

This appendix records methodological details for the solubility scenario-planning experiments in Section 5.3. The purpose is reproducibility and documentation.

I.1 Operational outcome definitions

Operational outcomes are defined in the main text via the binary prediction-set interface (Table 5). All reported quantities in the scenario-planning analysis are joint rates over the set-label outcomes $P(Y = y, C = c)$, scaled to expected counts over a window of $m = 1000$ molecules.

I.2 Pareto-front artifact and representative regimes

The full deduplicated Pareto front used in Section 5.3 is provided as a CSV artifact (`pareto_full.csv`). Each row corresponds to a distinct Pareto-optimal operating point after deduplication in KPI space. The CSV records (i) the SSBC effective levels $(\alpha_{\text{SSBC},0}, \alpha_{\text{SSBC},1})$, (ii) the nominal request parameters $(\alpha_0, \delta_0, \alpha_1, \delta_1)$ that induced the operating point, (iii) the six joint outcome rates $P(Y = y, C = c)$, and (iv) predictive-envelope endpoints for each joint rate (LB/UB), reported on the same probability scale and then converted below to counts per 1000.

Table 9 shows two representative Pareto regimes drawn from the provided Pareto front to illustrate contrasting planning postures: a loss-minimizing regime (low irreversible exclusion of soluble compounds) and a

Table 9: Two representative Pareto-optimal operating regimes for the solubility scenario, illustrating contrasting planning postures. Rates are expected counts per 1000 molecules, with predictive envelopes in brackets (derived from `pareto_full.csv`).

	Loss-minimizing regime		High-decisiveness regime	
α_0	0.125		0.150	
δ_0	0.150		0.150	
α_1	0.050		0.150	
δ_1	0.075		0.100	
	Rate	Interval	Rate	Interval
Loss rate	3	[0, 35]	12	[0, 58]
Waste rate	70	[27, 130]	13	[0, 49]
Total hedge rate	785	[663, 896]	514	[376, 675]
Correct soluble singleton rate	7	[0, 38]	88	[40, 155]
Correct insoluble singleton rate	135	[68, 215]	282	[196, 375]
Decisiveness (1 – hedge)	215		486	

decisiveness-maximizing regime (low total hedging). Counts are expected events per 1000 molecules; brackets denote the corresponding predictive envelopes.

1.3 Dataset and label construction

We use AquaSolDB as the source of aqueous solubility measurements ($\log S$), following the curation and quality-control procedures described in the dataset reference (Sorkun et al., 2019). For model training and scoring we discretize $\log S$ into three regimes with fixed thresholds: Insoluble ($\log S < -4$), Moderate ($-4 \leq \log S < -2$), and Soluble ($\log S \geq -2$), defining a three-class label space $\mathcal{Y} = \{0, 1, 2\}$ (Kalepu & Nekkanti, 2015).

1.4 Partitioning: scaffold-isolated training and exchangeable evaluation

We use a two-stage split to separate generalization across chemical space from the exchangeable design required for conformal calibration and finite-window operational analysis:

- **Scaffold grouping.** Molecules are grouped by Bemis–Murcko scaffolds (Bemis & Murcko, 1996) computed from RDKit (Landrum, 2025) SMILES.
- **Scaffold-isolated training set.** Scaffold groups are randomly shuffled and assigned to the training set until approximately 70% of molecules are allocated, ensuring no scaffold in training appears in the remaining pool.
- **Exchangeable calibration/test sets.** The remaining scaffold-disjoint molecules are split into calibration and test sets by a stratified random split (50/50 of the remaining pool), preserving class proportions. These two sets are treated as exchangeable with respect to each other and to future draws under the evaluation regime in Section 5.3.

1.5 Molecular representation

Molecules are represented using a fixed descriptor set supplemented with Morgan fingerprints (Rogers & Hahn, 2010). Representation is kept task-agnostic; no assay- or regime-specific feature engineering is performed. Molecules that fail parsing or yield invalid descriptor values are excluded.

1.6 Model and training protocol

We train a CatBoost (Prokhorenkova et al., 2018) gradient-boosted decision tree classifier on the scaffold-isolated training set with fixed hyperparameters (depth 6, learning rate 0.05, multi-class loss), up to 1000 boosting iterations with early stopping (patience 50) using calibration-set performance. After training, the predictor is frozen and treated as infrastructure; the experiments study the conformal and operational layers rather than optimizing base accuracy.

1.7 Calibration and operationalization

Uncertainty quantification uses split conformal prediction with SSBC calibration (Section 5.1.1 and Appendix C), which selects a grid index to stabilize realized coverage semantics at user-specified confidence (Vovk, 2012a; Yang & Kuchibhotla, 2021). This calibration layer supports the finite-window predictive-envelope constructions used for operational planning.

Although the classifier is trained on three classes (Insoluble, Moderate, Soluble), the planning analysis in Section 5.3 uses a binary operational objective obtained by merging Moderate and Soluble into a single Soluble class. Conformal prediction sets are computed in the binary label space {Insol, Sol} and operational quantities (loss, waste, hedging, decisiveness) are computed with respect to this binary interface.

1.8 Deployment-matched calibration via chemical tribes

Scenario planning conditions exchangeability on a deployment-defining event by restricting calibration to a chemically defined subpopulation.

Generic scaffold attribution. For interpretability we compute a generic scaffold representation by extracting the Murcko scaffold and converting it to a generic form (all atoms carbon, all bonds single). This increases scaffold group size and supports qualitative attribution across broader structural families.

Tribe construction. We define coarse chemical "tribes" using RDKit MolLogP:

$$\begin{aligned}\text{Tribe_Lipophilic} &: \text{MolLogP} > 3.5, \\ \text{Tribe_Hydrophilic} &: \text{MolLogP} < 1.0, \\ \text{Tribe_Neutral} &: 1.0 \leq \text{MolLogP} \leq 3.5.\end{aligned}$$

We compute summary statistics of nonconformity and class probabilities stratified by tribe on both the calibration pool and the held-out test window, and use these diagnostics to select a focal deployment regime.

Focal deployment scenario. Section 5.3 focuses on a lipophilic deployment regime. SSBC calibration is therefore performed on the restricted sample

$$\mathcal{D}_{\text{cal}}^{\text{lip}} = \{(X_i, Y_i) \in \mathcal{D}_{\text{cal}} : \text{MolLogP}(X_i) > 3.5\},$$

treated as exchangeable with respect to the intended deployment distribution.

Scenario-conditional exchangeability assumption. This restriction is scenario conditioning, not a general covariate-shift correction. We assume deployment draws satisfy the same scenario event $E = \{\text{MolLogP}(X) > 3.5\}$ so calibration and deployment are exchangeable conditional on E . If deployment violates E , or if exchangeability fails within E , conformal validity is not guaranteed. Shift-robust validity methods are complementary and outside scope; see, e.g., Fannjiang et al. (2022).

Interpretation. Conditioning trades calibration sample size for improved deployment match; the resulting loss of statistical efficiency appears directly as stronger SSBC corrections and wider predictive envelopes, consistent with transparent planning under finite-sample uncertainty.

I.9 Functional roles of calibration parameters

The Pareto sweep in Section 5.3 varies the four nominal parameters $(\alpha_0, \delta_0, \alpha_1, \delta_1)$ (with SSBC mapping them to effective deployed grid levels). Empirically the knobs are not interchangeable: changes reallocate mass among outcome categories (loss, waste, hedging, decisiveness) along channels constrained by the underlying threshold geometry.

Throughout, class 0 denotes insoluble and class 1 denotes soluble. The qualitative roles below summarize matched Pareto-optimal solutions where one parameter varies while the others are held fixed; rates are computed from the provided Pareto-front CSV and reported as events per 1000 molecules.

Role of α_0 : global conservatism against irreversible loss. Decreasing α_0 suppresses loss by expanding hedging; increasing α_0 collapses ambiguity into more decisive singleton predictions. In many matched segments, the dominant effect is redistribution between hedged and singleton outcomes with loss already near saturation.

Role of δ_0 : fine-scale sharpening on the insoluble side. For fixed $(\alpha_0, \alpha_1, \delta_1)$, δ_0 tends to act locally, shifting mass between hedged and singleton insoluble predictions with limited impact on loss.

Role of α_1 : boundary-controlled tolerance with nonlocal effects. Although α_1 is nominally associated with the soluble side, changing α_1 can move the operating point across geometric boundaries, inducing nonlocal reallocations that may appear most strongly in insoluble outcomes.

Role of δ_1 : systematic hedge-to-insoluble reassignment. Across stable regions of the front, increasing δ_1 often converts a portion of hedged mass into insoluble singletons, reflecting how the normalized score constraints and threshold geometry position the hedging interval.

Geometric interpretation. Overall, the Pareto front is shaped by geometric coupling rather than independent tuning: each knob reallocates probability mass along constrained channels determined by the threshold partition and the finite-sample SSBC adjustment.

I.10 Interpreting α versus δ on the Pareto front

Within SSBC the deployed threshold corresponds to an adjusted effective level $\tilde{\alpha}$ determined jointly by (α, δ) . Thus α and δ are best viewed as two parameterizations of a single underlying control (the effective threshold), with different practical resolution under finite-sample constraints. The approximate feasibility relation $\delta \approx (1 - \alpha)^N$ implies

$$\log \delta = N \log(1 - \alpha),$$

so changes in δ correspond to fine-grained (approximately logarithmic) adjustments in $\tilde{\alpha}$, whereas changes in α on a coarse grid can move the operating point across qualitatively different regions of the feasible manifold. This helps explain why α sweeps can trigger large reallocations among loss/waste/hedging outcomes, while δ sweeps more often act as local “sharpening” of decisions within a geometric regime.

References

- Anastasios N. Angelopoulos and Stephen Bates. Conformal prediction: A gentle introduction. *Foundations and Trends in Machine Learning*, 16(4):494–591, 2023. doi: 10.1561/2200000101.
- Anastasios N. Angelopoulos, Stephen Bates, Adam Fisch, Lihua Lei, and Tal Schuster. Conformal risk control. In *International Conference on Learning Representations*, 2024.
- Rina Foygel Barber, Emmanuel J. Candès, Aaditya Ramdas, and Ryan J. Tibshirani. Predictive inference with the jackknife+. *Annals of Statistics*, 49(1):486–507, 2021. URL <https://arxiv.org/abs/1905.02928>.

-
- Stephen Bates, Anastasios Angelopoulos, Lihua Lei, Jitendra Malik, and Michael I. Jordan. Distribution-free, risk-controlling prediction sets. *Journal of the ACM*, 68(6), September 2021. ISSN 0004-5411. doi: 10.1145/3478535. URL <https://doi.org/10.1145/3478535>.
- Guy W. Bemis and Mark A. Murcko. The properties of known drugs. 1. Molecular frameworks. *Journal of Medicinal Chemistry*, 39(15):2887–2893, 1996. doi: 10.1021/jm9602928.
- Michelle Bian and Rina Foygel Barber. Training-conditional coverage for distribution-free predictive inference. *Electronic Journal of Statistics*, 17(2):2044–2066, 2023. doi: 10.1214/23-EJS2145.
- George Casella and Roger L. Berger. *Statistical Inference*. Duxbury, 2nd edition, 2002.
- C. K. Chow. On optimum recognition error and reject tradeoff. *IEEE Transactions on Information Theory*, 16(1):41–46, 1970. doi: 10.1109/TIT.1970.1054406.
- H. A. David and H. N. Nagaraja. *Order Statistics*. Wiley, 2003.
- Aryeh Dvoretzky, Jack Kiefer, and Jacob Wolfowitz. Asymptotic minimax character of the sample distribution function and of the classical multinomial estimator. *Annals of Mathematical Statistics*, 27(3):642–669, 1956.
- Clara Fannjiang, Stephen Bates, Anastasios N. Angelopoulos, Jennifer Listgarten, and Michael I. Jordan. Conformal prediction under feedback covariate shift for biomolecular design. *Proceedings of the National Academy of Sciences*, 119(43):e2204569119, 2022. doi: 10.1073/pnas.2204569119. URL <https://arxiv.org/abs/2202.03613>.
- Seymour Geisser. *Predictive Inference: An Introduction*. Chapman and Hall, London, 1993.
- Isaac Gibbs, John J. Cherian, and Emmanuel J. Candès. Conformal prediction with conditional guarantees. *Journal of the Royal Statistical Society: Series B (Statistical Methodology)*, 87(4):1100–1126, 2025. doi: 10.1093/jrssi/bqkaf008. to appear.
- Ian Goodfellow, Yoshua Bengio, and Aaron Courville. *Deep Learning*. MIT Press, Cambridge, MA, 2016. ISBN 9780262035613.
- Wassily Hoeffding. Probability inequalities for sums of bounded random variables. *Journal of the American Statistical Association*, 58(301):13–30, 1963. doi: 10.1080/01621459.1963.10500830.
- Ruili Huang, Menghang Xia, Dac-Trung Nguyen, Jianying Zhao, Srilatha Sakamuru, Tingjun Zhao, Maxine Na, Swati A. Shahane, Anastasia Rossoshek, and Anton Simeonov. The tox21 data challenge to build predictive models of nuclear receptor and stress response pathways. *Nature Biotechnology*, 34(8):828–837, 2016. doi: 10.1038/nbt.3659.
- Norman L. Johnson, Samuel Kotz, and Narayanaswamy Balakrishnan. *Discrete Multivariate Distributions*. Wiley, New York, 1997. ISBN 978-0-471-31250-3.
- Sandeep Kalepu and Vijaykumar Nekkanti. Insoluble drug delivery strategies: review of recent advances and business prospects. *Acta Pharmaceutica Sinica B*, 5(5):442–453, 2015. doi: 10.1016/j.apsb.2015.07.003.
- Shayan Kiyani, George J. Pappas, Aaron Roth, and Hamed Hassani. Decision theoretic foundations for conformal prediction: Optimal uncertainty quantification for risk-averse agents. In *Forty-second International Conference on Machine Learning*, 2025. URL <https://openreview.net/forum?id=Ukj186EsIk>.
- Greg Landrum. RDKit: Open-source cheminformatics. <https://www.rdkit.org>, 2025. [Online; accessed 2026-02-13].
- Jing Lei, Max G’Sell, Alessandro Rinaldo, Ryan J. Tibshirani, and Larry Wasserman. Distribution-free predictive inference for regression. *Journal of the American Statistical Association*, 113(523):1094–1111, 2018. doi: 10.1080/01621459.2017.1307116.

-
- Jordan Lekeufack, Anastasios N Angelopoulos, Andrea Bajcsy, Michael I. Jordan, and Jitendra Malik. Conformal decision theory: Safe autonomous decisions from imperfect predictions. *arXiv preprint arXiv:2310.05921*, 2023.
- Paulo C. F. Marques. Universal distribution of the empirical coverage in split conformal prediction. *Statistics & Probability Letters*, 219:110350, 2025. ISSN 0167-7152. doi: 10.1016/j.spl.2024.110350. URL <https://www.sciencedirect.com/science/article/pii/S0167715224003195>.
- Pascal Massart. The tight constant in the dvoretzky–kiefer–wolfowitz inequality. *Annals of Probability*, 18(3):1269–1283, 1990. doi: 10.1214/aop/1176990746.
- Andreas Mayr, Günter Klambauer, Thomas Unterthiner, and Sepp Hochreiter. Deeptox: Toxicity prediction using deep learning. *Frontiers in Environmental Science*, 3:80, 2016. doi: 10.3389/fenvs.2015.00080.
- Kaisa Miettinen. *Nonlinear Multiobjective Optimization*. Kluwer Academic Publishers, Boston, 1999.
- Harris Papadopoulos, Kostas Proedrou, Volodya Vovk, and Alex Gammerman. Inductive confidence machines for regression. In Tapio Elomaa, Heikki Mannila, and Hannu Toivonen (eds.), *Machine Learning: ECML 2002*, volume 2430 of *Lecture Notes in Computer Science*, pp. 345–356. Springer, 2002. doi: 10.1007/3-540-36755-1_29.
- Liudmila Prokhorenkova, Gleb Gusev, Aleksandr Vorobev, Anna Veronika Dorogush, and Andrey Gulin. CatBoost: unbiased boosting with categorical features. In *Advances in Neural Information Processing Systems*, volume 31, pp. 6638–6648, 2018.
- David Rogers and Mathew Hahn. Extended-connectivity fingerprints. *Journal of Chemical Information and Modeling*, 50(5):742–754, 2010. doi: 10.1021/ci100050t.
- Yaniv Romano, Evan Patterson, and Emmanuel J. Candès. *Conformalized quantile regression*, pp. 1–11. Curran Associates Inc., Red Hook, NY, USA, 2019.
- Glenn Shafer and Vladimir Vovk. A tutorial on conformal prediction. *Journal of Machine Learning Research*, 9:371–421, 2008.
- Murat Cihan Sorkun, Abhishek Khetan, and Süleyman Er. Aqsoldb: a curated reference set of aqueous solubility and 2d descriptors for a diverse set of compounds. *Scientific Data*, 6:143, 2019. doi: 10.1038/s41597-019-0151-1. URL <https://www.nature.com/articles/s41597-019-0151-1>.
- Ryan J. Tibshirani, Rina Foygel Barber, Emmanuel J. Candès, and Aaditya Ramdas. Conformal prediction under covariate shift. In *Advances in Neural Information Processing Systems*, volume 32, 2019. URL <https://arxiv.org/abs/1904.06019>.
- Vladimir Vovk. Conditional validity of inductive conformal predictors. *arXiv*, 2012a. doi: 10.48550/arXiv.1209.2673. Extended version of ACML 2012 paper.
- Vladimir Vovk. Conditional validity of inductive conformal predictors. *Journal of Machine Learning Research*, 13:955–997, 2012b. URL <https://www.jmlr.org/papers/v13/vovk12a.html>.
- Vladimir Vovk. Cross-conformal predictors. *Annals of Mathematics and Artificial Intelligence*, 74:9–28, 2015. doi: 10.1007/s10472-014-9423-0.
- Vladimir Vovk, Alex Gammerman, and Glenn Shafer. *Algorithmic Learning in a Random World*. Springer, New York, 2005. doi: 10.1007/b106715.
- Fan Yang and Arun K. Kuchibhotla. Finite-sample efficient conformal prediction. *Annals of Statistics*, 49(5):2921–2947, 2021. URL <https://arxiv.org/abs/2104.13871v2>.
- Wenbin Zhou and Shixiang Zhu. Calibrating decision robustness via inverse conformal risk control. 2025. URL <https://arxiv.org/abs/2510.07750>.